CHARACTERIZATION OF THERMAL DAMAGE IN 2205 DUPLEX STAINLESS STEEL WITH NONLINEAR ULTRASONICS (NLU)

A Thesis
Presented to
The Academic Faculty

by

Thomas H. Ruiner

In Partial Fulfillment
of the Requirements for the Degree
Master of Engineering Science and Mechanics in the
School of Civil and Environmental Engineering

Georgia Institute of Technology
December 2010

CHARACTERIZATION OF THERMAL DAMAGE IN 2205 DUPLEX STAINLESS STEEL WITH NONLINEAR ULTRASONICS (NLU)

Approved by:

Dr. Laurence J. Jacobs, Advisor
School of Civil and Environmental Engineering
Georgia Institute of Technology

Dr. Jin-Yeon Kim
School of Civil and Environmental Engineering
Georgia Institute of Technology

Dr. Jianmin Qu
Department of Civil and Environmental Engineering
Northwestern University

Date Approved: November 11, 2010

ACKNOWLEDGEMENTS

It took a lot of great people to make my research work and my year in the U.S. so amazing. I'd like to express my sincere gratitude to all of them!

First of all, I'd like to thank my professor, adviser and friend, Dr. Laurence J. Jacobs, who always made time for me when I had questions or problems of any regard. I especially want to thank him for keeping this exchange program alive and making it possible for German students to spend an unbelievable year in the U.S.

Also, I absolutely want to express my gratitude towards Dr. Jin-Yeon Kim who spent a lot of time with me thinking about complicated problems I encountered during the course of my research. I owe him a lot, without his great advise and ideas this research would not have worked.

Special thanks go to Kevin Arne, who helped me polishing the specimens and with some other things. I really appreciate it!

Furthermore, I'd like to thank Prof. Dr.-Ing. Lothar Gaul from the Institut fuer Angewandte und Experimentelle Mechanik of the University of Stuttgart, Dipl.-Ing. Helge Sprenger, Katja Striegel of the Zentrum fuer Internationale Angelegenheiten and the Deutscher Akademischer Austausch Dienst (DAAD). All these people are involved in making this one and other exchange programs happen which is, in my opinion, something really important and valuable.

Of course, I'd also like to thank my friends and labmates Frank Bender, Dennis Schurr, Katie Matlack, Krzysztof Lesnicki and Sang Ryul Kim, who I had such a good time with, got academic input from and made the atmosphere in our lab so great.

Finally, my utmost gratefulness goes towards my family, who supported and encouraged me all the time.

TABLE OF CONTENTS

LIST OF TABLES

LIST OF FIGURES

SUMMARY

Duplex stainless steels have a microstructure that consists of almost equal shares of austenite and ferrite, which leads to excellent material properties. During production and processing, the steel can be exposed to high temperatures which leads to the development of a third (sigma) phase, and thus to a change in material properties.

The objective of this research is to assess the material damage in thermally degraded 2205 duplex stainless steel using nonlinear ultrasonics (NLU). Therefore, seven 2205 duplex stainless steel specimens are thermally degraded at 700°C for holding times up to 48 hours. The specimens are available only in one thickness and therefore, the propagation distance could not be varied which is causing difficulties. Preliminary nonlinear ultrasonic measurements revealed, that the error bars were so large that no conclusions could be drawn for the acoustic nonlinearity parameters of the specimens. If the propagation could be varied, constant influences like the transducers would basically cancel out and significantly more accurate results could be obtained.

For that reason, all sources for variation were investigated systematically and analyzed. From these investigations it is concluded, that the coupling condition is responsible for the variation of the measurements. An first improvement could be achieved by always applying the same amount of couplant, defined as the amount of a droplet that detaches by gravity from the needle of a syringe. With this procedure, the variation was almost reduced to half if a oil couplant was used, but the variation is still too high.

Based on these results, the transfer function is developed and the variation, which is due to the couplant, is described mathematically with the new equations. With

these equations, a correction method is proposed to correct the measurements by taking three additional correction measurements.

With the transfer function it could be shown that both, the transmitter and receiver are nonlinear. Furthermore, the transfer function makes it possible to eliminate the amplifier nonlinearity very efficiently, which is important if no low pass filter is used.

The final, uncorrected results for all specimen show a pattern that looks similar to the hardness plot. The diffraction correction factor, which is developed from only linear measurements, also shows a similar pattern. This makes it seem possible, that the differences between the nonlinearity parameters are actually related to something else than second harmonic generation in the material.

In order to calculate the fully corrected acoustic nonlinearity parameter, the nonlinearities of the transducers need to be known, but could not be measured with the equipment that was available for this research.

CHAPTER I

INTRODUCTION

1.1 Motivation

Steel is one of the most important materials for mankind. It is used all over the world in vehicles, ships, structures like bridges and skyscrapers, and many other applications. However, it is not always the same sort of steel, the various steel grades are very different concerning their material properties, such as strength, hardness and corrosion resistance. There are two basic principles of how these properties can be altered: By adding alloying elements or by using heat treatments such as annealing, quenching and tempering. Heat treatments are used to control grain size and phases in the steel.

During production and processing the steel can be exposed to high temperatures, which basically corresponds to an unwanted heat treatment. Depending on how high the temperatures are and how long the steel is exposed to them, the initial grain size and phase may be modified yielding to a change of material properties and maybe even malfunction and failure. Thus, after exposing steel to elevated temperatures, grain size and phase composition should be checked which is, however, very difficult to measure without destroying the sample. For that reason, a nondestructive method is needed to characterize changes in the material properties during thermal aging.

In this research thermally degraded 2205 duplex stainless steel specimens are studied using nonlinear ultrasonics. Nonlinear ultrasonics have shown high potential for characterizing material damage and microstructural changes due to various causes such as fatigue, creep and thermal aging [7],[2],[3],[1]. This raises hopes that the thermal damage in the specimens of this research can be quantified with nonlinear

ultrasonics.

1.2 Objectives

The objective of this research is to examine the potential of a longitudinal nonlinear ultrasonic technique to characterize thermal damage in 2205 duplex stainless steel. Therefore, seven specimens were thermally degraded at 700°C for different holding times in order to induce the thermal damage. Once the nonlinearity parameters are measured, it should be tried to relate potential differences to changes the microstructure of the specimens.

These nonlinear measurements turned out to have a standard deviation that was higher than differences between the acoustic nonlinearity parameters. Because of this, the objective was extended to investigate the influence of a high-power amplifier, transducers, and couplant on the nonlinear ultrasonic measurement and propose a method to correct for variations caused by them.

1.3 Structure of this Thesis

This thesis is structured as follows. Chap. 2 will briefly summarize the wave propagation concepts that are important for this research, especially the nonlinear wave propagation. After that, the experimental setup, procedure and the equipment will be introduced in Chap. 3. Chap. 4 addresses the problem of the large variation of the measurements, that make it difficult to distinguish a real difference of acoustic nonlinearity from a statistical fluctuation. Systematically all possible sources for this variation are examined and discussed. Based on these results, the transfer function is developed in Chap. 5 and the variation is mathematically described with the new equations. Furthermore, a way of correcting the measurements is proposed by taking three additional correction measurements. Chap. 6 utilizes the transfer function to investigate the influences of amplifier and transducers and shows that the transfer function works for this analysis. Finally, Chap. 7 shows and discusses the uncorrected

results for the nonlinearity parameter, the results of the correction measurements, and the final corrected nonlinearity parameter while Chap. 8 concludes this thesis with a conclusion and outlook.

CHAPTER II

TECHNICAL BACKGROUND

The equation of motion for a longitudinal planar wave is given by

$$\rho \frac{\partial^2 u}{\partial t^2} = \frac{\partial \sigma}{\partial x} \ , \tag{2.1}$$

where σ is the stress, x the propagation distance of the wave, u the displacement in x-direction, t the time, and ρ the material density. Furthermore, the simple form of Hooke's law is given by

$$\sigma = E \cdot \varepsilon \ , \tag{2.2}$$

where E the Young's modulus and ε the strain. However, this linear form is only valid for linear phenomena, not for nonlinear wave propagation. For nonlinear effects, Hooke's law can be extended by a power series expansion of strain,

$$\sigma = E\varepsilon(1 + \beta\varepsilon + \dots) \tag{2.3}$$

with β being the second order nonlinear coefficient ad thus, representing the material nonlinearity. With the strain - displacement relationship

$$\varepsilon(x,t) = \frac{\partial u(x,t)}{\partial x} \tag{2.4}$$

and Eq. 2.3 the equation of motion Eq. (2.1) can be rewritten as

$$\rho \frac{\partial^2 u}{\partial t^2} = E\frac{\partial^2 u}{\partial x^2} + 2E\beta \frac{\partial u}{\partial x}\frac{\partial^2 u}{\partial x^2} \ . \tag{2.5}$$

Assuming a perturbation solution, Eq. 2.5 can be solved [6],

$$\begin{aligned} U(x,t) =& A_1 cos(kx - \omega t) + A_2 sin(2(kx - \omega t)) \\ & - A_3 \Big[cos(3(kx - \omega t)) + cos(kx - \omega t) \Big] \end{aligned} \tag{2.6}$$

where A_i is the amplitude of the i-th harmonic wave, ω the frequency and k the wave number. Additionally, the second harmonic amplitude A_2 is given by

$$A_2 = \frac{A_1^2 k^2 x \beta}{8} \tag{2.7}$$

or rearranged

$$\beta = \frac{8 A_2}{x k^2 A_1^2} \ . \tag{2.8}$$

In the remainder of this research, the fundamental amplitude will be denoted as A^ω and the second harmonic correspondingly $A^{2\omega}$.

It can be noted, that the acoustic nonlinearity parameter β is proportional to three values, that can be measured rather easily: The fundamental and the second harmonic amplitude, as well as the propagation distance. With the new notation this gives

$$\beta \propto \frac{A^{2\omega}}{x \cdot (A^\omega)^2} \ . \tag{2.9}$$

Because of the limited bandwidth and frequency dependent sensitivity of transducers, a normal measurement will not yield absolute values for the amplitudes, but values that are proportional to the absolute ones. However, no absolute value for the acoustic nonlinearity parameter β is necessary to compare the seven specimens, because they are all measured with the same transducers and setup. In this case values that are proportional to the absolute value suffice, as given by

$$\beta' = \frac{A^{2\omega}}{x \cdot (A^\omega)^2} \ . \tag{2.10}$$

This β' is no longer an absolute value, which does not matter if different specimens are compared only quantitatively.

CHAPTER III

THE EXPERIMENT

3.1 2205 Duplex Stainless Steel Specimen

Duplex stainless steels have a duplex microstructure that consists of almost equal shares of ferrite (α) and austenite (γ). This leads to excellent material properties regarding strength, toughness and corrosion resistance[4],[5]. 2205 duplex stainless steel, the base material of this research, is one of the most widely used duplex stainless steel grades. During production and processing, the steel can be exposed to high temperatures which lead to the development of a sigma (σ)-phase, and thus to a change in material properties. As depicted in Fig. 3.1 the ferrite content decreases while the new sigma-phase basically transforms the ferrite into sigma-phase. The sigma-phase is very brittle and deteriorates the properties of the duplex stainless steel [10],[9].

Seven specimen measuring $25 \times 20 \times 12.1, mm^3$ were available for this research, all thermally aged at 700°C and quenched by water after the treatment. The holding

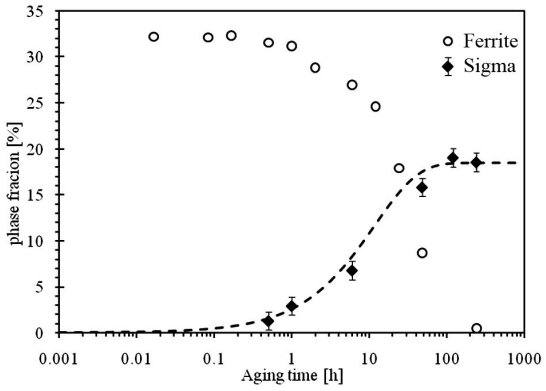

Figure 3.1: Ferrite Content with Respect to Holding Time at 700°C[8].

Table 3.1: Holding Times at 700°C for each Specimen.

Specimen	#1	#2	#3	#4	#5	#6	#7
Holding Time [min]	0	5	30	60	120	360	2880
Thickness [mm]	12.139	12.116	12.118	12.116	12.121	12.129	12.093

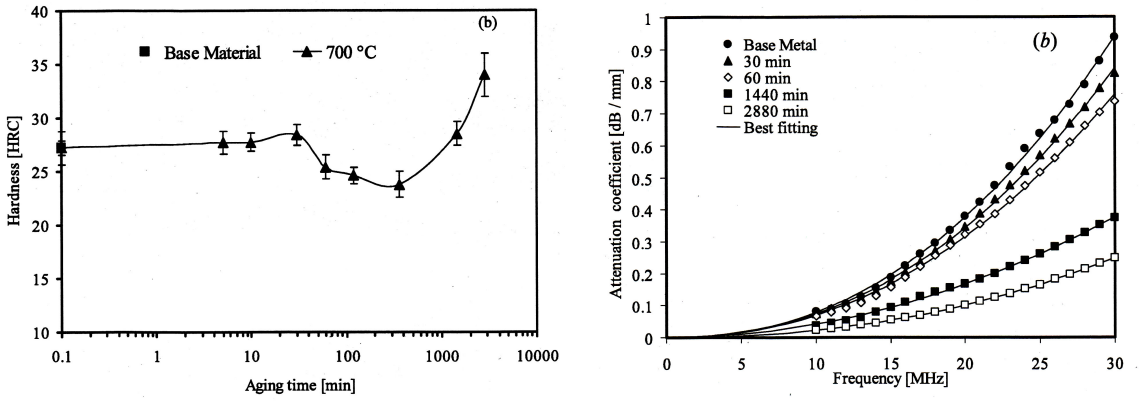

(a) Hardness

(b) Attenuation

Figure 3.2: Hardness and Attenuation with Respect to Holding Time at 700°C[8].

time for each specimen is listed in Table 3.1, as well as the exact thickness which varies 0.4%. Before the nonlinear measurements were started, all specimen were polished to ensure equal surface conditions.

Ruiz et al.[8] investigated the change in material properties, such as ferrite content, attenuation and hardness, of thermally degraded 2205 duplex stainless steel. The results are depicted in Fig. 3.1, and Fig. 3.2, respectively.

Furthermore, a microstructural analysis was conducted for different holding times. Fig. 3.3(a) shows the microstructure for a holding time of 10 minutes, in which the equal distribution of ferrite and sigma-phase can be seen. In addition to that, the development of new grain borders in the ferrite (white) can be observed in (a) and (b). After 6 hours holding time (c), considerable sigma precipitation can be noticed at the grain boundaries and finally, after 48 hours, the growing sigma-phase becomes dominant and only some remaining ferrite can be detected in (d).

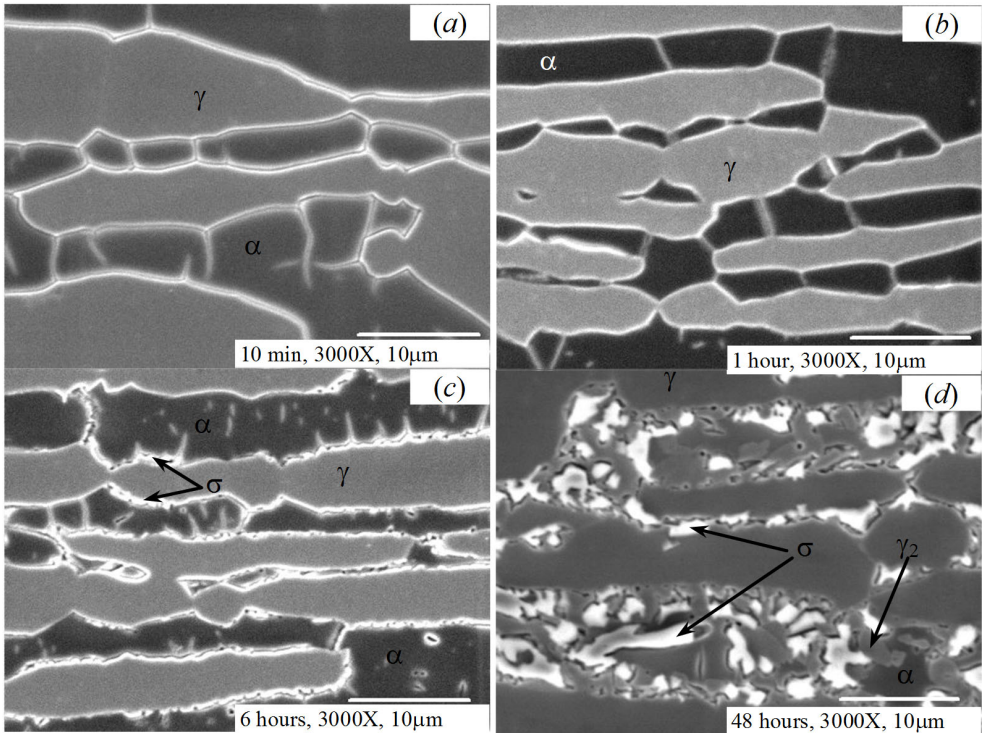

Figure 3.3: Microstructure of Thermally Aged 2205 Duplex Steel [8].

3.2 Instrumentation

3.2.1 Equipment

3.2.1.1 Signal Generation: RITEC RAM-5000 Amplifier

The RITEC RAM-5000 is a high power gated amplifier that creates sinusoidal tone bursts with up to 1.5 kW RMS output power. This amplifier type offers two advantages: Since the second harmonic amplitude is proportional to the square of the fundamental, the second harmonic becomes much more emphasized at higher output levels. This helps with the problem, that the second harmonic wave is usually very small and hard to detect within the fundamental wave and noise. The second advantage is the very clean sinusoidal wave, which excites the transmitter more linearly than a rectangular waveform. The detailed specifications of the RITEC RAM-5000 can be found in Table 3.2.

Table 3.2: Specifications RITEC RAM-5000

Frequency Range for Synthesizer	50 kHz to 22 MHz
Nominal Frequency Range for Gated Amplifier	250 kHz to 17.5 MHz
Nominal Output Impedance of Gated Amplifier	50 Ω
On/Off Ratio of Gated Amplifiers	< 140 dB
Output Level Control	< 20 dB
Typical Gated Amplifier RMS Output Power	1.5 kW between 0.25 and 7 MHz
Maximum Pulse Width	200 microseconds
Maximum Duty Cycle	0.3 %

3.2.1.2 Signal Generation: Agilent 33250A Function Generator

The Agilent 33250A is an arbitrary function generator with an maximum output of 10 V peak-to-peak. It was used for linear measurements when the high power of the RITEC RAM-5000 was not needed, because the RITEC RAM-5000 creates a more distorted waveform when used at low output levels.

3.2.1.3 Filter: RITEC FDK-5-10

The FDK-5-10 Diplexer is meant for nonlinear echo measurements with a fundamental frequency of 5 MHz. It consists of a 5 MHz Low Pass Filter (LPF) between amplifier and transducer to eliminate higher harmonics in the input signal and a 10 MHz High Pass Filter (HPF) between transducer and oscilloscope to increase the precision when measuring a second harmonic wave of 10 MHz. Both filters can be used independently and were utilized for the through transmission measurements in this research.

3.2.1.4 PZT Transducers

PZT stands for piezoelectric transducer and is the most commercial transducer type. It is acoustically very efficient but also very nonlinear. PZTs were used in the beginning of this research because these are easier to handle and more likely to be used as a field application. Also, the transducer's nonlinearity does not matter if the material

nonlinearity is considerably higher or when the wave propagation distance is varied. In the latter case the transducer nonlinearity ends up being only a constant. The PZTs used in this research were two narrow band transducers built by Olympus:

- Transmitter: Panametrics X1056, 5 MHz, 0.5"'
- Receiver: Panametrics A111S, 10 MHz, 0.5"

The 10 MHz receiver used in this research emphasizes the second harmonic but is still very responsive at 5 MHz and can detect fundamental wave reliably, as well.

3.2.1.5 Lithium Niobate Transducers

Lithium Niobate ($LiNbO_3$) transducers are single crystals and, unlike PZT, very linear. These crystals are difficult to handle, break easily and need to be glued onto the specimen. After the gluing process one has to solder wires onto the crystal to excite it. Valpey Fisher, a company situated in Massachusetts, builds custom made Lithium Niobate transducers by mounting the single crystals in a transducer case. These transducers are depicted in Fig. 3.4 and can be handled as easily as commercial PZTs. For this research a 5 MHz transmitter and 10 MHz receiver were used.

Figure 3.4: Valpey Fisher Lithium Niobate Transducers.

3.2.1.6 Tektronix P2100 100 MHz Voltage Probe

A voltage probe enables one to measure voltages accurately without disturbing the measured signal too much. This is ensured by a impedance of 10 MΩ which means almost no additional load to the amplifier. Also, it attenuates the signal by 20 dB which makes it possible to measure high voltages.

Over the course of this research the voltage probe was used to measure the driving high voltage input signal from the amplifier into the transmitter, but it can also be used to measure the echo of the ultrasonic wave.

3.2.1.7 Signal Acquisition: Oscilloscope

The Tektronix TDS 420 was used in the beginning of this research. Even at optimized settings the signal averaging speed never exceeds 30 Hz and it takes about 30 s to transfer the recorded signal onto the computer. Using higher sampling rates, higher signal averages or more than one channel is used at the same time, the averaging speed drops below 5 Hz. Under these circumstances, it can take more than 5 minutes to save results on the computer.

Once two and three channels were needed simultaneously, the Tektronix TDS 5034 Digital Phosphor Oscilloscope was used. With it, saving a recorded signal is almost instantaneous and the averaging speed does not decrease as drastically when more channels or a higher sampling rate are used. The really limiting factor is the repetition rate the transmitter can take from the amplifier. A measurement with three channels, a 1024 average and at a repetition rate of only 30 Hz took less then a minute, the TDS 420 could not handle these settings and crashed. Fig. 3.5 shows the Tektronix TDS 5034 with the two HPF stages in front of it.

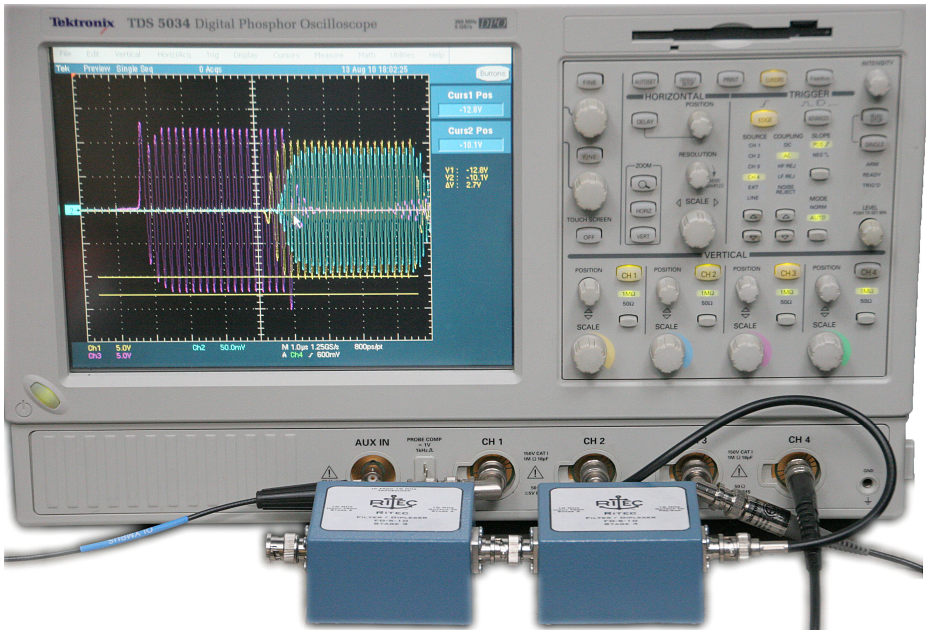

Figure 3.5: Tektronix TDS 5034 and HPF.

3.2.2 Home-Made Devices

3.2.2.1 High Power 50 Ω Termination

When a 50 Ω term has to withstand the high power signal generated by the RITEC RAM-5000, a couple of aspects have to be considered:

- The maximum output of the RITEC RAM-5000 is 4.5 W. However, these 4.5 W are the average of a 1500 W tone burst at the maximum duty cycle of 0.3%, so the peak power is considerably higher. For that reason, a long lasting 50 Ω termination should be able to sustain more than just 4.5 W. This can be accomplished by either using better resistors or by building parallel circuits and therefore, splitting the power.

- The voltage of the RITEC RAM-5000 was measured to be as high as 2000 V peak-to-peak into a 50 Ω load, and up to 800 V peak-to-peak with a Lithium Niobate transducer attached. Thus, the electrical devices need to sustain this voltage. This can be accomplished by using appropriate resistors or building a

series circuit, in which case the voltage is split.

- Wire wound resistors cannot be used because of their inductance. Tests showed that the signal will either be distorted or just not improve very much.

- Wires without shielding should be avoided and the leads on the resistors should be as short as possible or otherwise the waveform will be distorted.

The 50 Ω termination was inserted between amplifier and transducer using a T-piece, as shown in Fig. 3.6. That way, there are no unshielded cables directly between transducer and amplifier.

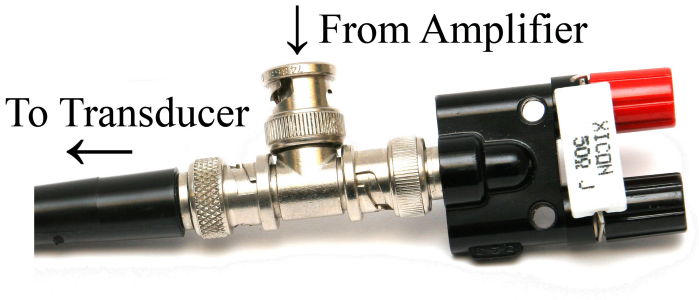

Figure 3.6: Home-Made 50 Ω Termination.

3.2.2.2 Fixture

The fixture aligns the two transducers exactly on the same axis. It clamps the specimen and allows removing one transducer without disturbing the coupling condition on the other one. Micrometer screws with rounded ends compensate for angular discrepancies and allow precise force application. In order to apply a constant pressure on the back of the transducer, a small metal plate with a piece of rubber glued to it is put between micrometer screw and transducer. The rubber compensates for the transducer's uneven back and works as a very stiff spring.

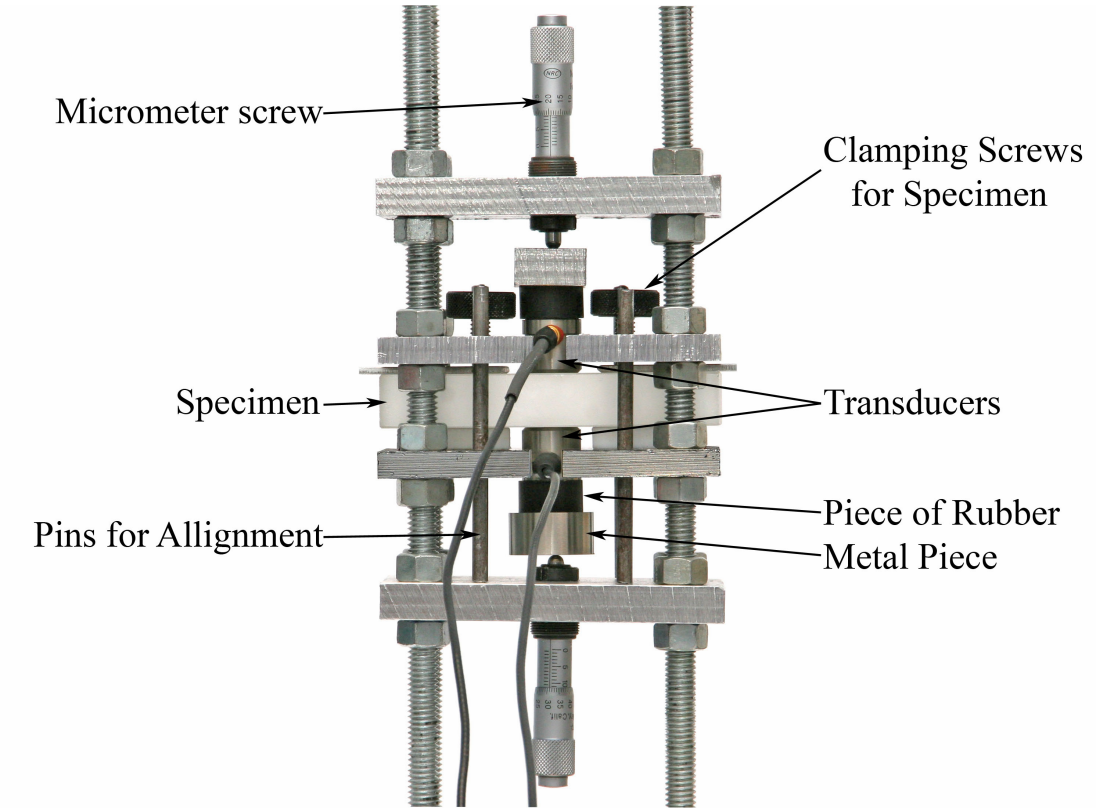

Figure 3.7: Home-Made Fixture for Nonlinear Measurements.

3.3 Experimental Setup and Procedure

Fig. 3.8 shows a schematic of the experimental setup used in this research. Fig. 3.8(a) illustrates the setup for the nonlinear measurements, in which the high power gated amplifier generates a sinusoidal 5 MHz tone burst with 21 cycles. 21 is the number of cycles that can be excited before the echo of the first cycle arrives back at the transmitter and might cause adverse nonlinear influences by reflections and wave interference. The electrical signal from the amplifier is terminated with 50 Ω and low pass filtered to block all frequency components higher than 5 MHz. Then the filtered signal excites the 5 MHz transducer which is clamped onto the specimen using the fixture from Chap. 3.2.2.2. The ultrasonic wave is measured by the 10 MHz receiver on the opposed side of the specimen. The 10 MHz receiver emphasizes the second

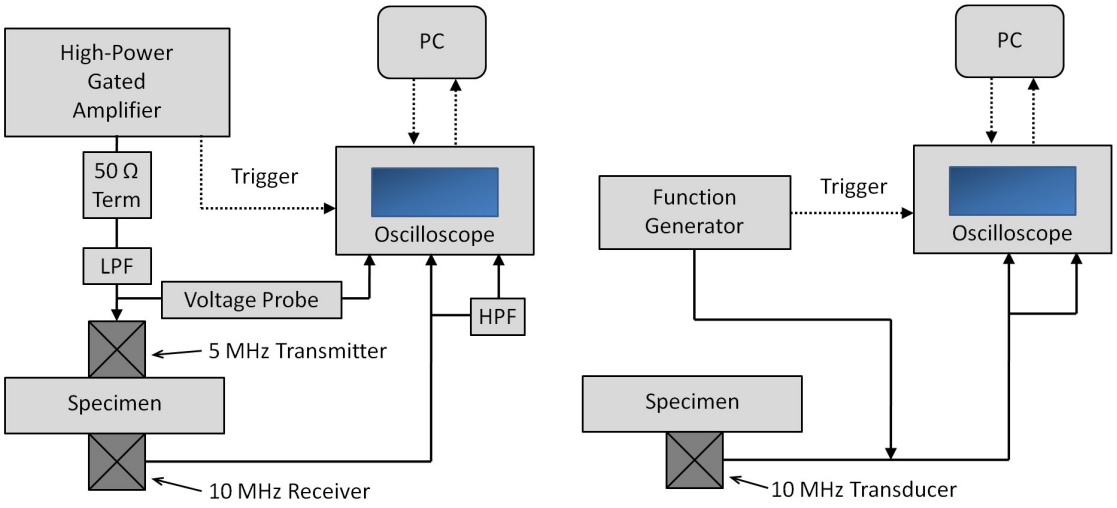

(a) Nonlinear Through Transmission (b) Linear Echo Measurement

Figure 3.8: Experimental Setup.

harmonic component of the ultrasonic wave but is still very responsive to the fundamental wave, therefore both can be measured reliably. The signal at the receiver is measured with the oscilloscope using two channels simultaneously, one for the direct and one for the high pass filtered signal. Furthermore, 1024 signals are averaged with the oscilloscope to improve the signal to noise ratio (SNR).

Fig. 3.8(b) shows the setup for the echo measurements with the 10 MHz transducer, which is used to correct the nonlinear measurements. The signal is generated by a function generator because no high power is needed. Furthermore, it is measured by the oscilloscope using two channels simultaneously. One channel is set to measure the electrical input signal, the other one is set to measure the echo.

In the beginning of this research all experiments were conducted using a couplant oil, but it was discovered and described in Chap. 4.4.2 that the lower viscosity of water makes it possible to obtain good results much faster. The way how and how much couplant is applied to the transducer can influence the results significantly,

Figure 3.9: Couplant

especially with the oil coupling. For that reason, a technique was developed to keep the amount of couplant always similar: Couplant was filled into a syringe and carefully pressed through the needle, until one droplet detaches by gravity from the needle, as illustrated in Fig. 3.9. Then both transducers are pressed together and moved in a circular motion to distribute the couplant equally over the surface. With this technique, the initial variation of the measurements was almost reduced to half when a couplant oil was used. For water this procedure did not make a difference.

The *individual technique,* meaning how one sets up the specimen, applies couplant and pressure, has a large influence on the results. For that reason, after every experiment a different specimen is used for the next experiment. That way gradual changes in the technique affect all specimens equally.

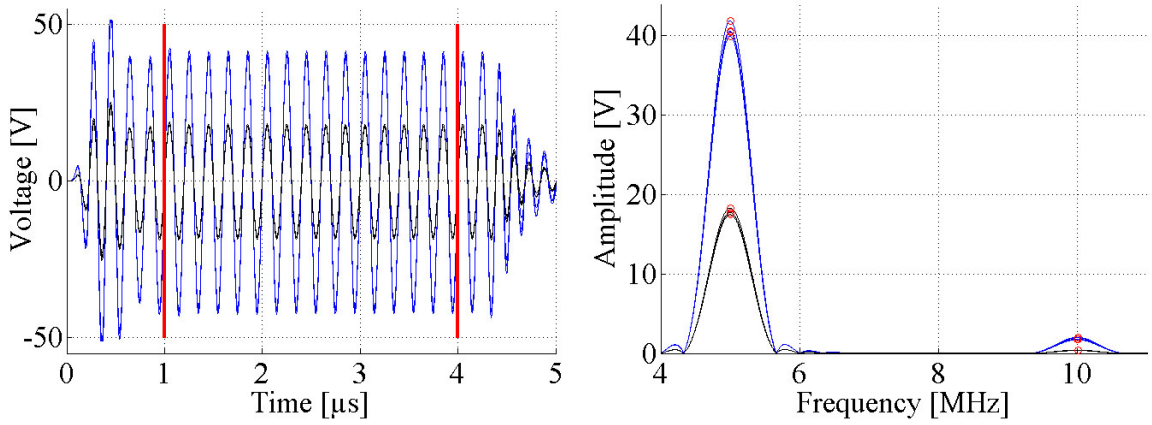

(a) Steady-State Portion (b) Frequency Spectrum

Figure 3.10: Raw Signal and Calculated Frequency Spectrum

3.4 Signal Processing

Only the steady-state portion of the measured signal, illustrated by the red lines in Fig. 3.10(a), is used for the data processing. The window is picked in such a way, that the first point of the window is the first positive value of a beginning sine wave, and the last point the last negative value of a ending sine wave. Then a Hann-window is applied to enhance the results of the Fast Fourier Transform (FFT), which is used to obtain the frequency spectrum of the signal and illustrated in Fig. 3.10(b). Combined with zero-padding, this procedure gives good results for the fundamental and second harmonic amplitudes. More details about the influence of a Hann-window and zero-padding can be found in Chap. 4.2.5.

CHAPTER IV

ANALYSIS OF VARIATION OF NONLINEAR MEASUREMENTS

4.1 Motivation

The preliminary measurements that were conducted with the steel specimens revealed clear tendencies for the nonlinearity parameter β - but they turned out to be false. An increased repetition rate increased the amplifier's nonlinearity giving tendencies for the material nonlinearity that just did not exist. The amplifier is not the only origin for false results: The *individual technique*, meaning how one sets up the specimen, applies couplant and pressure, has a large influence on the results as well. No significant change of the individual technique is necessary, a gradual change of how the couplant is applied and the transducer mounted will yield a gradual change of the nonlinearity parameter, disguising actual differences between the specimen.

Once a way was found to keep the individual technique and all settings constant, another problem came up: Consecutive measurements of the same specimen varied by up to $\pm 20\%$, while the differences between the specimen seemed to be much smaller. Under these circumstances there was no way to quantify the nonlinearity parameter β of the seven steel specimen.

For this reason, a thorough investigation was conducted to find possible sources of error and a way to avoid or compensate them, with the ultimate goal to obtain the nonlinearity parameters of the steel specimen and correlate these to the thermal damage.

4.2 Data Acquisition and Signal Processing

This chapter addresses influences that are only due oscilloscope settings and data processing in Matlab.

4.2.1 Variation of Transmitter Input Voltage

The best way to accurately measure the nonlinearity parameter β is to vary the wave propagation distance x, because system nonlinearities are independent of the propagation distance. Therefore, the difference between measurements with different propagation distance is due to material nonlinearity only. The propagation distance of the ultrasonic wave remains constant in this research because the specimens are available only in one thickness. Also, the thickness is smaller than the transducer's diameter and thus, wave propagation in width or length direction could not be used for measurements.

Instead of varying the propagation distance, one can also vary the amplitude of the fundamental wave. This gives additional data points for each measurement and a best fit line can be used to improve the accuracy. The amplitude can be changed in two ways: Either by changing the output level of the amplifier or by using an attenuator. Three nonlinear measurements on steel where conducted to find out if several output levels improve the accuracy. Fig. 4.1 shows the variation of the second harmonic with respect to the output level. It is obvious, that the second harmonic generated by the amplifier is a function of the output level and always has the same characteristic. Thus, using several output levels does not improve the accuracy. Since varying the output level one could think using an attenuator might improve the results. Experiments have shown that two consecutive measurements differ by less than 0.1% if the setup is not changed. This means, that the one measurement is already precise enough and consequently, only one data point per measurement was aquired in this research.

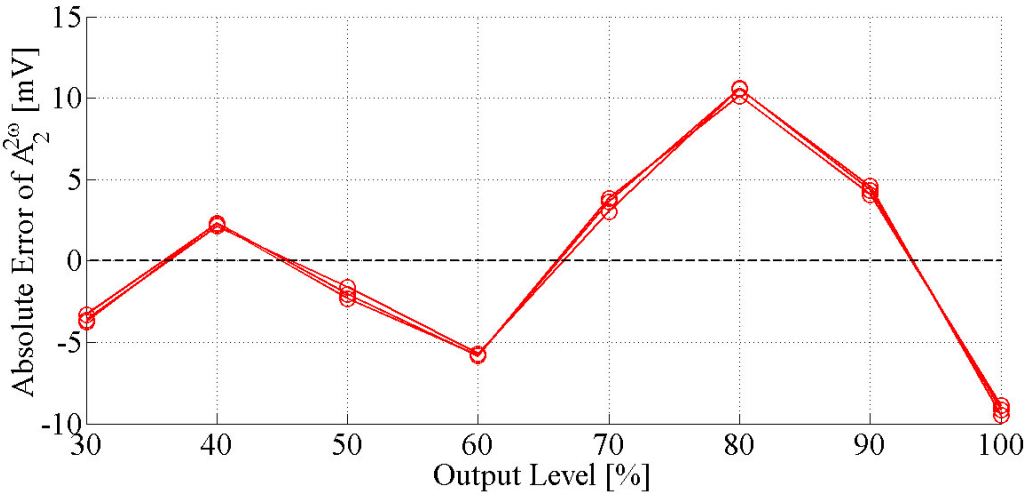

Figure 4.1: Variation of Second Harmonic around Best Fit Line.

4.2.2 Signal Averaging

When the amplifier is used at an output level of 90% the oscilloscope measures a 40 V amplitude of the fundamental frequency with both, the PZT and Lithium Niobate receivers which gives a very high signal to noise ratio (SNR). If the material is, like steel, very nonlinear then the SNR is also very good for the second harmonic. Experiments showed that for these conditions a 64 average is already sufficient. Still, a 1024 average was used if not indicated otherwise. That way the amplitude of the fundamental can be reduced and less nonlinear specimen can be measured without.

4.2.3 Sampling Rate

The sampling rate is basically the resolution of the x-axis or time-axis. The Nyquist rate is the minimum sampling rate and equals twice the highest frequency of interest. The highest frequency that is interesting in this study is 10 MHz which yields a minimum sampling rate of 20 MHz or 20 $\frac{MS}{s}$. In order to rule out that the variation of the measured values is due to a low sampling rate, a convergence study was performed. Therefore, an identical signal was measured by the receiver using different sampling rates. Then the measured amplitudes of the fundamental and the second harmonic

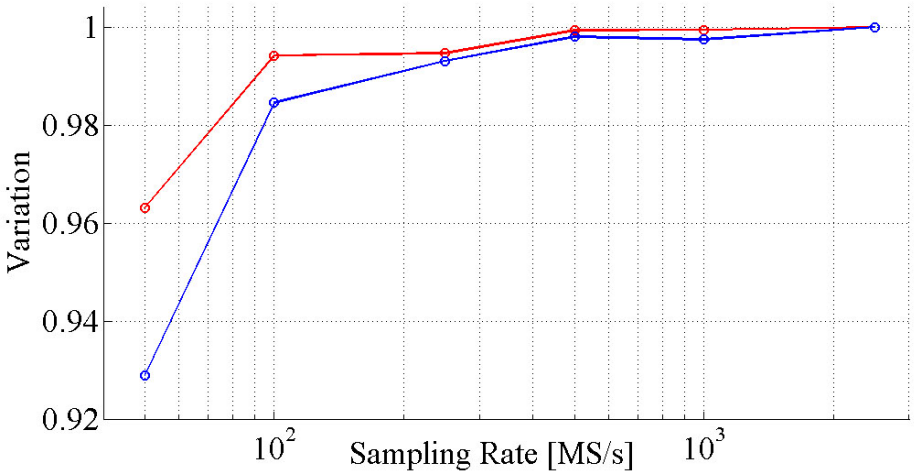

Figure 4.2: Convergence Study of the Sampling Rate.

waves, A^{ω} and $A^{2\omega}$, were plotted with respect to the sampling rate, shown in Fig. 4.2. It can be observed that the values seem to converge to a certain value for higher sampling rates, which intuitively makes sense.

If a lower sampling rate is simulated by dropping data points of a measured data set, the convergence plot looks very similar and thus, confirms the measured convergence study. Based on these results all experiments were conducted using a sampling rate of 500 $\frac{MS}{s}$ or higher to ensure consistency and accuracy.

Remarks

The convergence study does not necessarily mean that lower sampling rates will cause variation. It is also possible that the values are always identically too low and then not any worse.

4.2.4 Resolution of the Y-Axis

The sampling rate, which was discussed in the previous chapter, basically describes the resolution of the time or x-axis. The vertical y-axis refers to the measured voltage and every digital oscilloscope has a limited resolution for the y-axis which must not

be underestimated. The resolution can only be adjusted to the measured signal in rather large steps, so that sometimes one ends up recording a signal that only fills half of the screen and thus, uses only half of the oscilloscope's full dynamic range. This is sufficient for the fundamental frequency which is visible on the screen, the second harmonic however can be as little as 0.5% of the fundamental wave, for example, in the measurement on Borosilicate. In this case the results are subject to variation only due to the lack of sufficient resolution.

This effect is illustrated in Fig. 4.3. Notice that not only the accuracy, but also the absolute values and slope are different. By comparing results of different resolutions it can be shown that the values converge and thus, in order to get consistent and especially repeatable results, it is important to use the full dynamic range of the oscilloscope. This problem can be avoided if a HPF is used, which is described in Chap. 4.3.4.

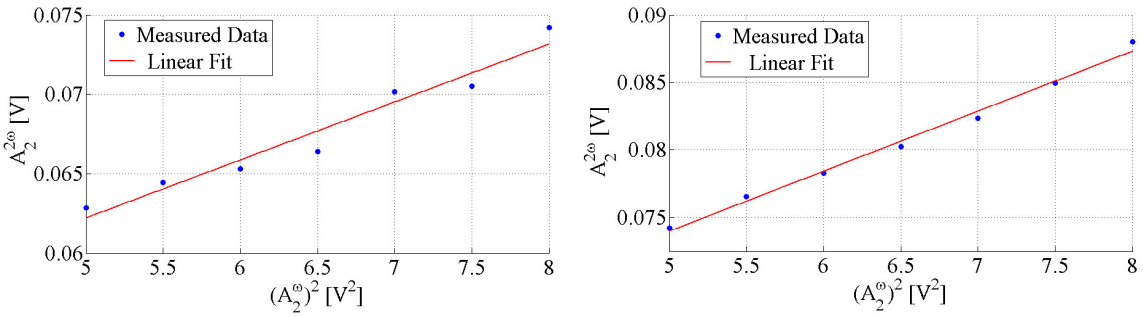

(a) Insufficient Resolution (b) Maximum Resolution

Figure 4.3: Influence of the Y-Axis Resolution on Nonlinear Measurements.

4.2.5 Zero Padding and Hann Window

In this section two ways of improving the results by data processing are analyzed. On the one hand **zero padding** which increases the resolution of FFT by adding zeros to the time domain signal. The **Hann window** on the other hand emphasizes the center of the signal. Fig. 4.4(a) shows the receiver signal of a through transmission

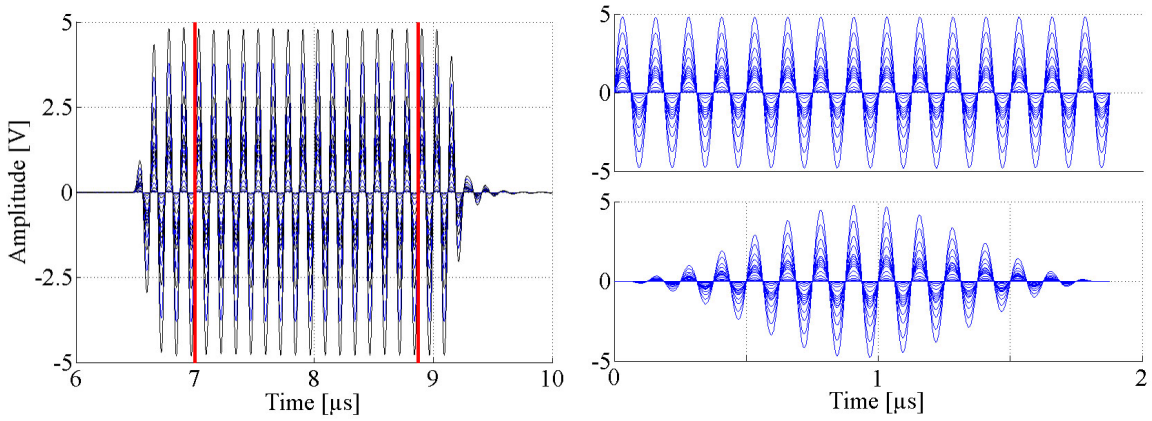

(a) Receiver Signal (b) Applied Windows

Figure 4.4: Measured Signal and Applied Windows

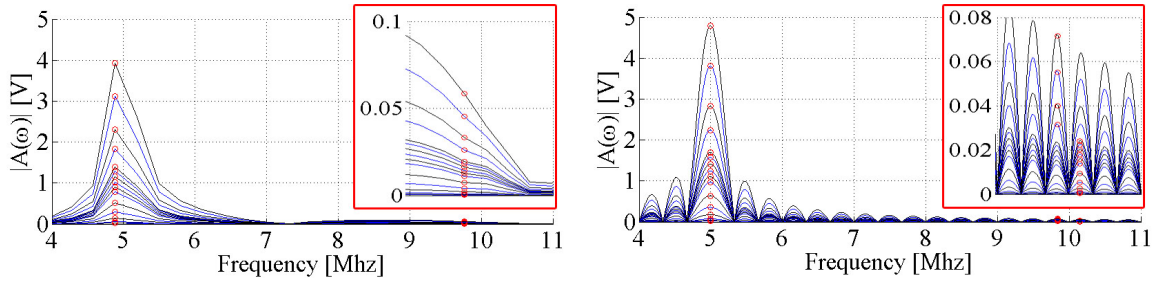

(a) Rectangular Window Only (b) Additional Zero Padding

Figure 4.5: Rectangular Window and Zero Padding

experiment on Borosilicate. Several measurements were taken with different fundamental amplitudes and a sampling rate of $500\frac{MS}{s}$, which is 25 times the Nyquist rate. A rectangular window and Hann window are applied on the steady-state portion of the waveform between the two red lines, the result is depicted in Fig. 4.4(b). After the window functions are applied, a FFT can be used to obtain the frequency spectrum of the signal. Figs. 4.5 and 4.6 show the influence of zero padding if the FFT is applied on the rectangular window and Hann window, respectively. The red box within the figures illustrates the second harmonic using a different scale. With these results a few conclusions can be drawn:

- The rectangular window without zero padding is useless. The FFT yields neither the correct amplitude for the fundamental, nor for the second harmonic

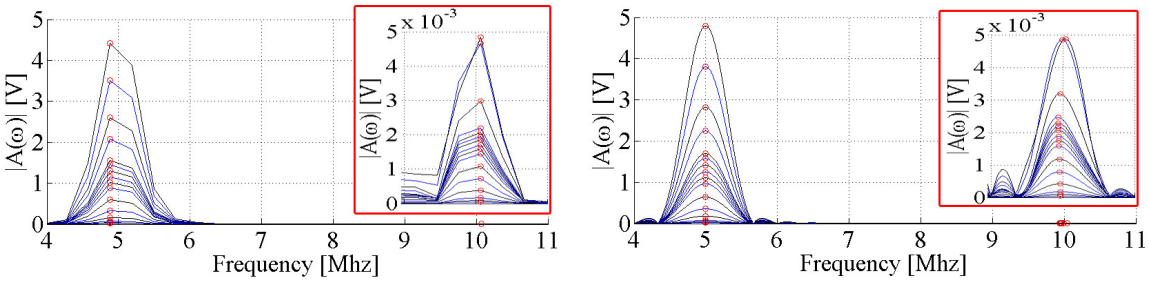

(a) Hann Window Only

(b) Additional Zero Padding

Figure 4.6: Hann Window and Zero Padding

frequency.

- The rectangular window with zero padding gives accurate results for the fundamental frequency. However, the second harmonic is completely hidden in the FFT side effects.

- The Han window without zero padding yields good results for the second harmonic, but the values for fundamental amplitude are wrong and the frequency resolution is insufficient.

- Only the Han window with zero padding gives good results. The frequencies for fundamental and second harmonic are very precise and the amplitude values are correct for the fundamental and good for the second harmonic frequency. The latter were confirmed by an additional measurement with a HPF.

If a smaller window length is used, and therefore just the very center of the steady-state portion of the waveform in Fig. 4.4(a), the FFTs without zero padding yield correct values for the fundamental amplitude as well. However, this is not enough data to get decent values for the second harmonic. Thus, it can be concluded, that a Hann window and zero padding are needed to obtain good values from the FFT.

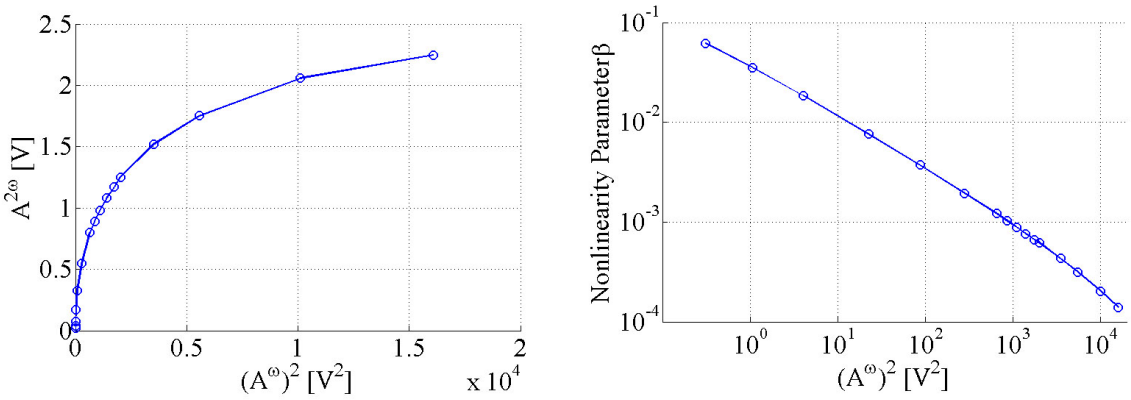

(a) RITEC Nonlinearity

(b) RITEC Nonlinearity Parameter β

Figure 4.7: Amplifier Nonlinearity

4.3 Equipment Influences

In this chapter the influences of the equipment is analyzed that was used in this research.

4.3.1 Amplifier

The gated amplifier used in this research and introduced in Chap. 3.2.1.1 creates a sinusoidal signal with the fundamental frequency but this electrical signal is already contaminated with higher harmonics. This means that the transmitter will convert these electrical higher harmonics into mechanical waves, even if the transmitter itself is linear. How big an influence this has depends obviously on how linear the amplifier and how broadband the transmitter is. Using the PZT transmitter on borosilicate the amplifier can actually make up more than 50% of the overall second harmonic. Fig. 4.7 (a) shows the second harmonic in the electrical signal of the amplifier with an Lithium Niobate Transducer attached and Fig. 4.7 (b) the relative nonlinearity parameter $\beta = \frac{A^{2\omega}}{(A^{\omega})^2}$. It is obvious, that The amplifier is more nonlinear at lower output levels, so the effect can be reduced by working at higher output levels. Also, the effect is less important if the material is very nonlinear and it can be almost be

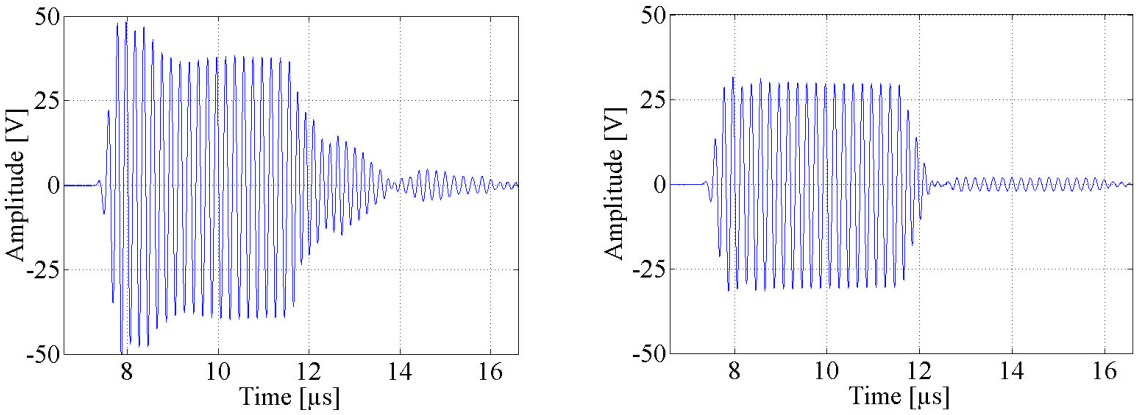

(a) Distorted Waveform (LPF only)

(b) Improved Waveform (LPF and 50 Ω Term)

Figure 4.8: Waveform with LPF and 50 Ω Term.

completely eliminated by using a LPF, as shown in Chap. 4.3.3. The effect can also be canceled out using additional correction measurements and data processing. The procedure is explained in Chap. 6.1.

4.3.2 50 Ω Termination

RITEC, the manufacturer of the amplifier, recommends using a 50 Ω term at the output because the amplifier has a 50 Ω impedance and works best when it sees a 50 Ω load. Using a 50 Ω term at the amplifier and a PZT transmitter the measured nonlinearity of a steel specimen decreased by about 10%. This may be caused by the amplifier creating a cleaner signal or the 50 Ω term absorbing a higher percentage of higher harmonics.

Furthermore, the 50 Ω term improves the waveform if the load is mismatched from 50 Ω, as shown in Fig. 4.8.

4.3.3 Low Pass Filter (LPF)

The 5 MHz LPF attenuates frequencies higher than 5 MHz significantly. This is of great importance if the amplifier is very nonlinear and the transmitter is sufficiently responsive to the 10 MHz component of the input signal. The RITEC 5 MHz LPF

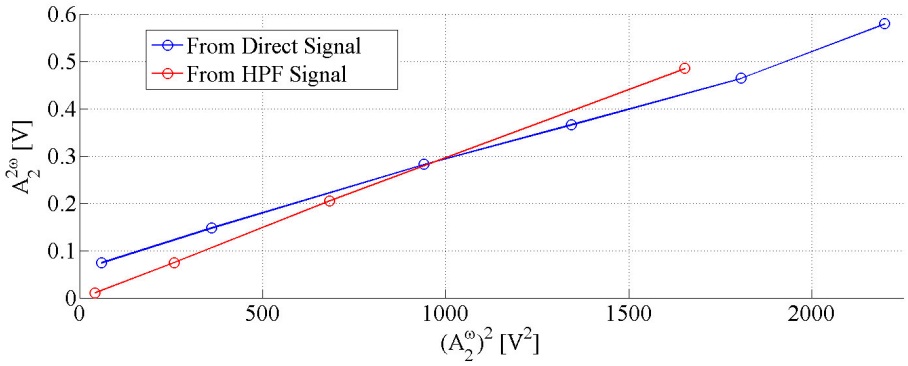

Figure 4.9: Influence of the Low Pass Filter(LPF).

was found to reduce the 10 MHz component in the input signal by roughly 99%. The effect can be seen in Fig. 4.9, a measurement on Borosilicate with PZT transducers. The plots should yield a straight line according to $\frac{A^{\omega}}{(A^{\omega})^2}$, which is only the case if the LPF is used. The reasons for how the curves are shaped is explained in Chap. 6.1.

The impedance of the LPF is different from 50 Ω and therefore the waveform is distorted as shown in Fig. 4.8. However, a 50 Ω Term improves the waveform considerably.

4.3.4 High Pass Filter (HPF)

The 10 MHz HPF is used on the receiver side to filter the fundamental 5 MHz signal out, and it is more than 99.99% efficient in doing so. This helps visualizing the second harmonic on the oscilloscope and improves the results significantly if the second harmonic is very small. In this case the fundamental would saturate the oscilloscope and one would get variations that are only due to oscilloscope's resolution as described in Chap. 4.2.4. Using the HPF the second harmonic signal can be isolated, amplified and measured reliably.

Fig. 4.10 shows the improvement for a measurement of a Borosilicate specimen using different output levels. Borosilicate is very linear and thus, the second harmonic very small. Ideally, the nonlinearity parameter should give the same value for each

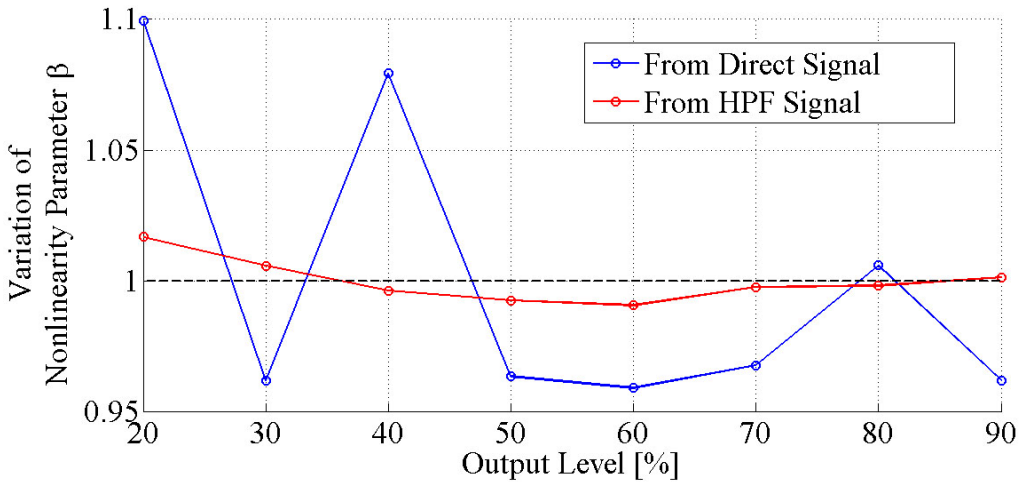

Figure 4.10: Influence of the High Pass Filter(HPF).

out level, but under these circumstances the y-axis resolution of the oscilloscope is not high enough for measurements without HPF, which can be seen from the inconsistent nonlinearity parameter. However, when the HPF is used, a very smooth and constant line is obtained. The increasing nonlinearity parameter for lower output levels confirms the higher amplifier nonlinearity at lower output levels, which was already described in Chap. 4.3.1. Another proof of how much the HPF improves the results can be seen in Chap. 6.1.

4.3.5 Transducers

How a transducer influences the nonlinear measurement depends on if it is used as a transmitter or receiver.

4.3.5.1 Transmitter

The transmitter influences the nonlinear measurements in two ways. The first one is the transmitter's nonlinearity which will be measured by the receiver as well, distorting the measured material nonlinearity. The second aspect is how well the transmitter responds to a second harmonic signal from the amplifier. If the transmitter did not respond to a second harmonic signal at all, then the amplifier nonlinearity, which was

discussed in Chap. 4.3.1, would not be converted into a mechanical wave and thus, not matter.

4.3.5.2 Receiver

For the receiver it is only important how nonlinear it is. Even though the amplitude at the receiver is smaller than at the transmitter, it still creates a considerable amount of nonlinearity which is shown in Chap. 6.2.3. The proof requires the transfer function, which will be established in Chap. 5.

4.4 Mechanical Influences

This chapter analyses influences, that are due to the way, the equipment is utilized by the user.

4.4.1 Heating of the Amplifier and Load Change

Heating of the high power amplifier occurs after turn-on but also when the load is changed, in which case cooling is also a possibility. This is important because the amplifier's nonlinearity is temperature dependent and the influence of it must not be underestimated. In the beginning of this research specimens 1,2 and 7 were measurement and specimen 7 was found to be roughly 10% more nonlinear than the others. This increased nonlinearity was only due to a different amplifier setting. The amplifier was set to a higher repetition rate to accelerate the data acquisition which meant a higher load.

Fig. 4.11 shows how the fundamental and second harmonic amplitudes during the heating after turn-on. The values were obtained from a nonlinear measurement and it can be seen that $(A^{\omega})^2$ and $A^{2\omega}$ change in a similar pattern. This means, that the ratio, which is proportional to the nonlinearity parameter β does not vary as much.

There are two practical ways to decrease the amplifier influence. First of all, the heating time after turn-on can be reduced significantly if a higher duty cycle is used.

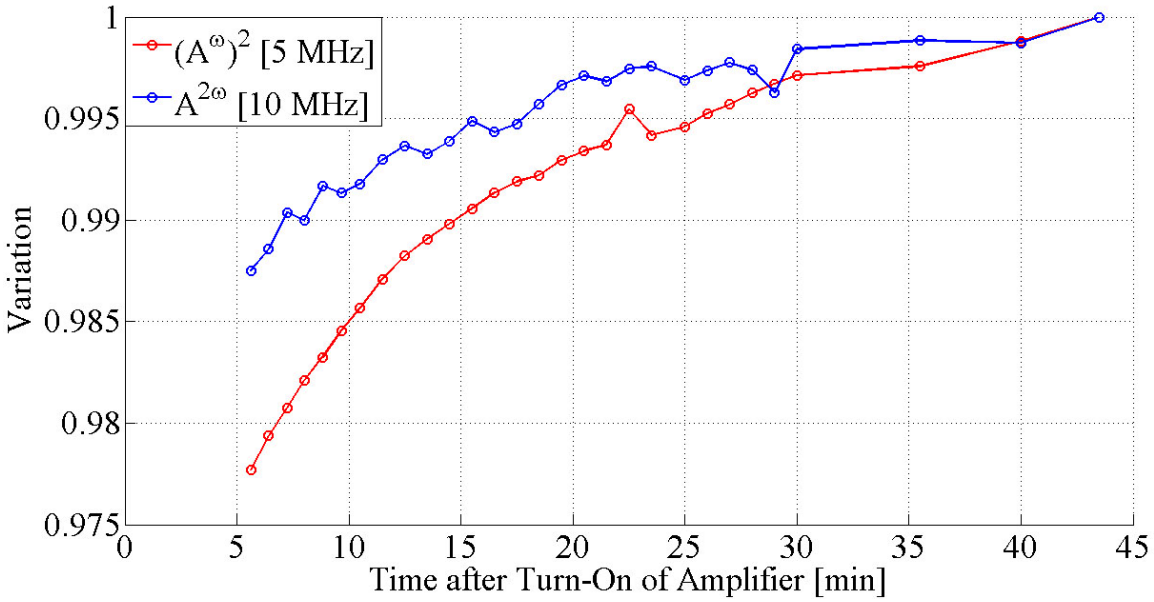

Figure 4.11: Heating of the Amplifier.

For example, after 8 minutes at 100 Hz the temperature for measurements with a 20 Hz repetition rate is reached. Secondly, the temperature dependent nonlinearity can be removed using a LPF as described in Chap. 4.3.3.

4.4.2 Relaxation Processes

After the specimen and transducers are mounted changes in the measured amplitudes can be observed. This may be due to changes in the couplant layer and some elastic relaxation in the fixture. The shape of the relaxation curves cannot be predicted and may look different from the example depicted in Fig. 4.12. The fundamental and second harmonic amplitudes may change inversely as shown in the plot, in a similiar manner, or even not change at all. The most frequently observed and worst case is the inverse behavior, because this gives the largest change of the nonlinearity parameter $\beta \propto \frac{A^{2\omega}}{(A^{2\omega})^2}$.

Further investigation showed, that it can take up to 20 minutes until the amplitudes have fully converged. However, the relaxation process is only partly the reason for the variation of the nonlinear measurements, since the amplitudes converge to

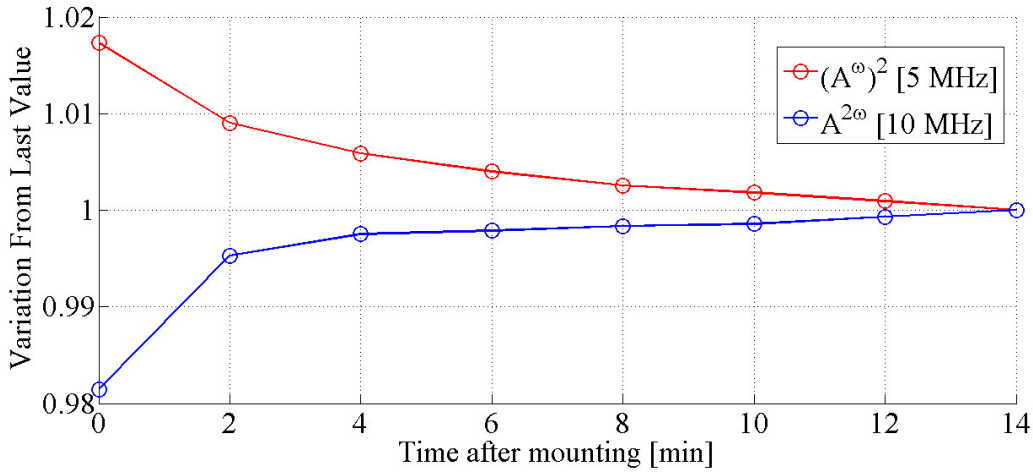

Figure 4.12: Relaxation Process.

different values each time.

Fig. 4.12 was obtained using the same couplant oil, that was used for most experiments of this research. Just before the final nonlinear measurements of all seven specimens were conducted, another experiment revealed that the relaxation process is mainly due to the viscosity of the couplant. Using very viscous glycerin the relaxation process persisted considerably longer, while ordinary water showed almost no relaxation. Therefore, water was used for the ultimate measurements of the steel specimens.

4.4.3 Clamping Force

After all influences which were described in the previous chapters are ruled out, only the couplant and coupling force are left as possible reasons for the large variation of the measurements. In order to find the reason for the variation an experiment with four sets of measurements was conducted, each set consisting of two measurements. The transducers were mounted onto the specimen normally and one basic measurement was taken. Then the clamping force was increased or decreased, such that a certain amplitude of the fundamental frequency was reached.

The results are shown in Fig. 4.13. It is obvious, that the differences between the

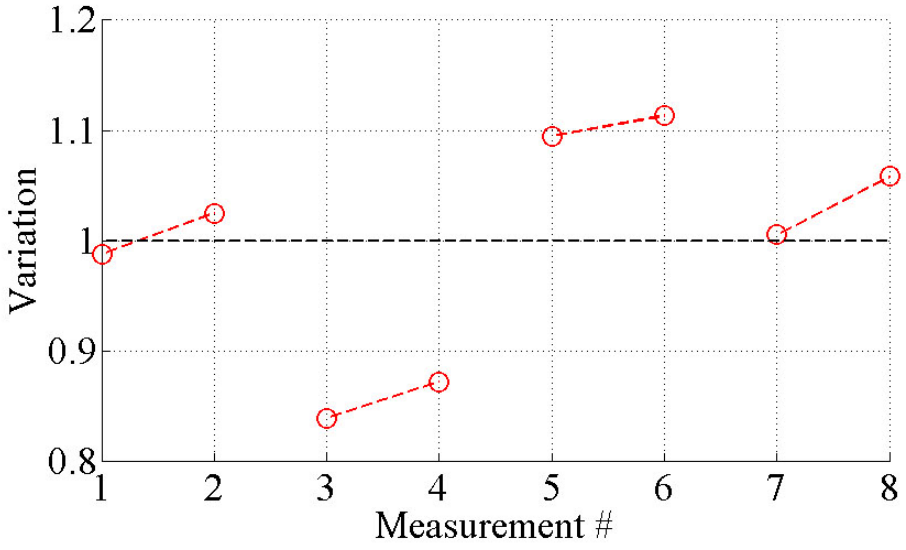

Figure 4.13: Influence of Force Change.

sets outweigh the differences within the sets by far. Thus, the coupling condition has the most influence on the variation. With this knowledge it can also be suspected that the variation within the sets is due to changes in the couplant condition, which are induced by the coupling force.

4.4.4 Couplant Layer

The couplant layer can influence nonlinear measurements in two ways. First of all, it could be nonlinear and actively generate a second harmonic wave. However, it seems likely that the nonlinearity does not vary a lot and therefore, probably does not cause the large variation of the nonlinear measurements. The second way to influence the measurement is by varying transmission coefficients for the fundamental and second harmonic waves. Even if both transmission coefficients are reduced equally by 10%, then the ratio $\frac{A^{2\omega}}{(A^{\omega})^2}$ changes by $\frac{0.9}{0.9^2}$ or 11%.

The transmission coefficient can be measured and used to correct the results, but this cannot be done without identifying all sources of nonlinearity. The necessary analysis is performed in the next chapter.

Apart from that, by applying the couplant with a syringe as described in Chap. 3.3 the initial variation could almost reduced to half for oil couplants.

CHAPTER V

TRANSFER FUNCTION TO MODEL SYSTEM NONLINEARITIES

The transfer function is used to describe the relationship between the electrical input signal that excites the transmitter and the electrical output signal from the receiver. This knowledge makes it possible to isolate certain influences, such as coupling conditions, and is the basis for making corrections to the nonlinear measurements in this research. The transfer function is is similar to an approach that was proposed by Sun et al. [11]. However, the correction method that was proposed is different and did not yield improvement for the results.

5.1 Linear Measurements

The common reference configuration for all measurements is the experimental setup for the nonlinear through transmission experiment. Side 1 is defined as the side, where the transmitter is placed for the nonlinear measurement and this transmitter is defined as transducer 1. This is important because transducer 1 can also be used as a receiver. Summarized, the numbers 1 and 2 refer to the position in the nonlinear experiment, while the words *transmitter* and *receiver* explain the current purpose.

The main idea of the transfer function is, that the wave propagation process can be split into several steps. Therefore, two functions need to be explained:

- Conversion function G: Describes how efficiently a transducer converts the electrical signal into a physical wave or the other way round.
- Transmission coefficient T: Describes how much of a incoming wave is transmitted through a couplant layer.

Both are complex numbers that not only describe amplitude relations, but also possible phase shifts. A procedure how all transmission coefficients can be measured was already suggested by Treiber et al.[12].

5.1.1 Through Transmission

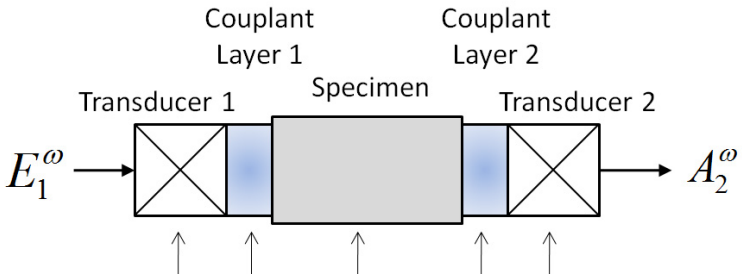

$$E_1^\omega \quad \cdot \quad \left(G_{1,t}^\omega \cdot T_{1,t}^\omega \cdot D_x^\omega \cdot T_{2,r}^\omega \cdot G_{2,r}^\omega\right) = A_2^\omega \tag{5.1}$$

- E_1^ω: Electrical sinusoidal signal of frequency $\boldsymbol{\omega}$ from the amplifier that drives transducer **1**.
- $G_{1,t}^\omega$: Conversion function at a frequency $\boldsymbol{\omega}$ of transducer **1**, working as a **T**ransmitter. Thus, an electrical signal is turned into a physical wave.
- $G_{2,r}^\omega$: Conversion function at a frequency $\boldsymbol{\omega}$ of transducer **2**, working as a **R**eceiver. Thus, a physical wave is turned into an electrical signal.
- $T_{1,t}^\omega$: Transmission coefficient on side **1**, wave propagation from **T**ransmitter into material at a frequency $\boldsymbol{\omega}$.
- $T_{2,r}^\omega$: Transmission coefficient on side **2**, wave propagation from material into **R**eceiver at a frequency $\boldsymbol{\omega}$.
- D_x^ω: Diffraction coefficient for a wave that propagates a distance $\boldsymbol{x}$ at a frequency $\boldsymbol{\omega}$.
- A_2^ω: Electrical signal of frequency $\boldsymbol{\omega}$ that is measured by transducer **2**.

5.1.2 Echo Measurements

The transfer function for echo measurements with one transducer and one free surface can be derived easily from the through transmission function of the previous chapter, Eq. (5.1). Therefore, total reflection is assumed where the other transducer used to be and the transmitting transducers works as a receiver for the reflected wave.

$$-E_1^\omega \cdot \left(G_{1,t}^\omega \cdot T_{1,t}^\omega \cdot D_{2x}^\omega \cdot T_{1,r}^\omega \cdot G_{1,r}^\omega\right) = A_1^\omega \tag{5.2}$$

5.2 Nonlinear Through Transmission Measurements

The measured second harmonic wave is actually the superposition of several second harmonic waves of different origins, such as material, transducers, and amplifier. This makes it more complicated to describe a nonlinear measurement with the transfer function because every source of nonlinearity has to be considered individually.

5.2.1 Derivation of the Transfer Function

The derivation in this chapter analyses how the driving electrical input signal finally yields the second harmonic that is measured by the receiver. For that purpose the next chapters follow the propagation of the fundamental wave and chronologically consider second harmonic generation in every of the following six steps:

	Wave after:	Notation:
1.	Input (Amplifier)	A_i^ω
2.	Transmitter	A_t^ω
3.	Transmitter-Couplant	A_{c1}^ω
4.	Material	A_m^ω
5.	Receiver-Couplant	A_{c2}^ω
6.	Receiver	A_2^ω

The notation depicted above will make the derivation of the transfer function clearer.

One assumption is made before hand:

- Second harmonic generation outside the material occurs according to $\alpha \propto \frac{A^{2\omega}}{(A^{\omega})^2}$.

Transducer crystals and especially couplant layers are very thin, which means there is almost no wave propagation distance x. According to Eq. (2.9), $\left(\beta \propto \frac{A^{2\omega}}{x \cdot (A^{\omega})^2}\right)$, the nonlinearity of these thin layers would need to be impossibly high to cause any noticeable effect. Especially since the steel specimens are already quite nonlinear and the propagation distance is several decimal powers higher. Consequently, if transducers and couplant are taken into account, then it makes sense to assume a second harmonic generation that is somewhat independent of the propagation distance. Experiments show that the relationship $\frac{A^{2\omega}}{(A^{\omega})^2} = const.$ still holds true, which can be seen in Fig. 4.9: Once the amplifier nonlinearity is filtered out, the relationship holds true despite of the other nonlinearities in the system. Thus, a nonlinearity parameter α is introduced to describes the nonlinearity of transducers and couplant layers: $\alpha \propto \frac{A^{2\omega}}{(A^{\omega})^2}$.

5.2.1.1 Input

An ideal amplifier creates a perfectly shaped sinusoidal signal of one single frequency that excites the transmitter. In reality, amplifiers never create such a clean signal. Thus, the electrical input signal that drives the transmitter, is already contaminated with a second harmonic:

$$\text{Linear:} \quad A_i^{\omega} = E_1^{\omega} \tag{5.3}$$

$$\text{Nonlinear:} \quad A_i^{2\omega} = E_1^{2\omega} \tag{5.4}$$

5.2.1.2 Transmitter

The second harmonic component in the electrical signal (Eq. (5.4)) will excite the transmitter and form a physical wave. Mathematically this process can be described

by multiplying with the conversion function $G_{1,t}^{2\omega}$. Aside from this process, the transmitter is primarily excited at the fundamental frequency, transforming the electrical signal into physical movement. With the transmitter oscillating at the fundamental frequency a second harmonic oscillation is created according to $\alpha_1 \propto \frac{A^{2\omega}}{(A^{\omega})^2}$ because of the transducer nonlinearity. This means that another second harmonic wave is generated and that already two independent second harmonic waves propagate from the transmitter to the receiver at this point.

$$\text{Linear:} \quad A_t^{\omega} = G_{1,t}^{\omega}\, A_i^{\omega} \tag{5.5}$$

$$\text{Nonlinear:} \quad A_t^{2\omega} = \alpha_1 \left(G_{1,t}^{\omega}\, A_i^{\omega}\right)^2 + G_{1,t}^{2\omega}\, A_i^{2\omega} \tag{5.6}$$

5.2.1.3 Transmitter Couplant

The two second harmonic waves $A_t^{2\omega}$ that are coming from the transmitter are influenced by couplant through the transmission coefficient only: $T_{1,t}^{2\omega}\, A_t^{2\omega}$.

If second harmonic generation in the couplant layer is considered a few assumptions have to be made. Since the couplant layer is of a finite thickness the linear transmission coefficient actually consists of two transmission coefficients, one for the front and one for the back side of the couplant layer. It is assumed, that these two transmission coefficients are about the same, which yields

$$T_{1,t}^{\omega} \approx \sqrt{T_{1,t}^{\omega}}\sqrt{T_{1,t}^{\omega}}. \tag{5.7}$$

In the next step, second harmonic generation in the couplant layer is assumed to work the following way: The fundamental wave enters the couplant layer with the transmission coefficient $\sqrt{T_{1,t}^{\omega}}$. Inside, a second harmonic is generated and leaves the couplant with the transmission coefficient $\sqrt{T_{1,t}^{2\omega}}$. This yields overall:

$$\text{Linear:} \quad A_{c1}^{\omega} = T_{1,t}^{\omega}\, A_t^{\omega} \tag{5.8}$$

$$\text{Nonlinear:} \quad A_{c1}^{2\omega} = \sqrt{T_{1,t}^{2\omega}}\alpha_{c1}\left(\sqrt{T_{1,t}^{\omega}}\, A_t^{\omega}\right)^2 + T_{1,t}^{2\omega}\, A_t^{2\omega} \tag{5.9}$$

5.2.1.4 Material

The second harmonics which were created before the material, are only influenced by the diffraction coefficient: $D_x^{2\omega}\, A_{c1}^{2\omega}$.

Apart from that, a second harmonic is generated by the fundamental wave propagating through the material according to Eq. (2.10),[1] $\beta' = \frac{A^{2\omega}}{x \cdot (A^{\omega})^2}$. Since the second harmonic amplitude increases linearly with the propagation distance, the second harmonic generation can be thought of as an accumulation of infinitesimal portions of second harmonics, that are created along the way. Thus, some second harmonic components are created later than others. This means, that neither D_x^{ω} nor $D_x^{2\omega}$ correctly describe the diffraction for a second harmonic, that is, for example, created in the middle of the material. The correct diffraction coefficient is defined as $D_x^{\omega-2\omega}$.

An approximation of $D_x^{\omega-2\omega}$ can be derived: For a portion of second harmonic, that is created right after the fundamental wave enters the material, only $D_x^{2\omega}$ is relevant. For another portion of second harmonic, that is created right before the fundamental leaves the material, $D_x^{2\omega}$ does not matter anymore. But the fundamental had to propagate all the way through the material before and therefore, was influenced by D_x^{ω}.

Now consider a portion of second harmonic, that is created on neither side but right in the center of the material and assume that the diffraction coefficient can be split similarly to the transmission coefficient in the previous chapter:
$D_x^{\omega} = \sqrt{D_x^{\omega}}\,\sqrt{D_x^{\omega}}$. The fundamental wave propagated only half the overall distance before the second harmonic is created and the diffraction coefficient is assumed to be $(D_x^{\omega})^{\frac{1}{2}}$. The second harmonic that is created in the center only needs to propagate half the distance as well, and the diffraction coefficient is approximated by $(D_x^{2\omega})^{\frac{1}{2}}$. Mathematically, the second harmonics of these three exemplary points can be written

[1] Note that this β' is not an absolute value. This does not matter if different specimen are compared quantitatively as described in Chap. 2.

Creation point Second harmonic

as $\bar{x} = 0 \cdot x$: $A^{2\omega} = (D_x^{2\omega})^1 \beta_m \Big((D_x^{\omega})^0 A^{\omega} \Big)^2$

$\bar{x} = \frac{1}{2} \cdot x$: $A^{2\omega} = (D_x^{2\omega})^{\frac{1}{2}} \beta_m \Big((D_x^{\omega})^{\frac{1}{2}} A^{\omega} \Big)^2$

$\bar{x} = 1 \cdot x$: $A^{2\omega} = (D_x^{2\omega})^0 \beta_m \Big((D_x^{\omega})^1 A^{\omega} \Big)^2$.

An equation for an arbitrary position $\bar{x}$ within the material can be found by interpolating between these three points above:

$$\bar{x} = \frac{\bar{x}}{x} \cdot x : \qquad A^{2\omega} = (D_x^{2\omega})^{1-\frac{\bar{x}}{x}} \beta_m \Big((D_x^{\omega})^{\frac{\bar{x}}{x}} A^{\omega} \Big)^2 \tag{5.10}$$

The overall second harmonic that is created by the material can be calculated using Eq. 5.10 and integrating over the material thickness x:

$$\begin{aligned} A^{2\omega} &= \beta_m \, (A^{\omega})^2 \int_0^x (D_x^{2\omega})^{1-\frac{\bar{x}}{x}} (D_x^{\omega})^{2\frac{\bar{x}}{x}} \, d\bar{x} \\ &= \beta_m \, (A^{\omega})^2 \, x \, \underbrace{\frac{(D_x^{\omega})^2 - D_x^{2\omega}}{2\ln(D_x^{\omega}) - \ln(D_x^{2\omega})}}_{D_x^{\omega - 2\omega}} \end{aligned} \tag{5.11}$$

Thus, an approximation for the diffraction coefficient $D_x^{\omega-2\omega}$ is obtained:

$$D_x^{\omega-2\omega} \approx \frac{(D_x^{\omega})^2 - D_x^{2\omega}}{2\ln(D_x^{\omega}) - \ln(D_x^{2\omega})} \tag{5.12}$$

Apart from that, the second harmonics, that were created before the material, are only influenced by the diffraction coefficient. Both findings combined yield

$$\text{Linear:} \quad A_m^{\omega} = D_x^{\omega} \, A_{c1}^{\omega} \tag{5.13}$$

$$\text{Nonlinear:} \quad A_m^{2\omega} = \, x \, \beta_m \, D_x^{\omega-2\omega} \, (A_{c1}^{\omega})^2 + D_x^{2\omega} \, A_{c1}^{2\omega}. \tag{5.14}$$

5.2.1.5 Receiver Couplant

The events in the receiver couplant are completely analogous to the transmitter couplant.

$$\text{Linear:} \quad A_{c2}^{\omega} = T_{2,r}^{\omega} \, A_m^{\omega} \tag{5.15}$$

$$\text{Nonlinear:} \quad A_{c2}^{2\omega} = \, \sqrt{T_{2,r}^{2\omega}} \, \alpha_{c2} \, \left(\sqrt{T_{2,r}^{\omega}} \, A_m^{\omega} \right)^2 + T_{2,r}^{2\omega} \, A_m^{2\omega} \tag{5.16}$$

5.2.1.6 Receiver

The fundamental wave excites the receiver at the fundamental frequency, which yields an additional second harmonic oscillation if the receiver is nonlinear. This second harmonic, together with the second harmonic waves that enter the receiver through the couplant layer, are transformed into a electrical signal by the conversion function $G_{2,r}^{2\omega}$.

$$\text{Linear:} \quad A_2^{\omega} = G_{2,r}^{\omega}\, A_{c2}^{\omega} \tag{5.17}$$

$$\text{Nonlinear:} \quad A_2^{2\omega} = \; G_{2,r}^{2\omega} \left(\alpha_2 \, (A_{c2}^{\omega})^2 + A_{c2}^{2\omega} \right) \tag{5.18}$$

By expanding Eq. (5.18) the different sources of nonlinearity and their contribution can be seen:

$$\begin{aligned}
A_2^{2\omega} = \; & G_{2,r}^{2\omega}\, \alpha_2 \left(T_{2,r}^{\omega}\, D_x^{\omega}\, T_{1,t}^{\omega}\, G_{1,t}^{\omega}\, E_1^{\omega} \right)^2 && \text{(Receiver)} \\
& + G_{2,r}^{2\omega} \sqrt{T_{2,r}^{2\omega}}\, \alpha_{c2}\, T_{2,r}^{\omega} \; \left(D_x^{\omega}\, T_{1,t}^{\omega}\, G_{1,t}^{\omega}\, E_1^{\omega} \right)^2 && \text{(Couplant 2)} \\
& + G_{2,r}^{2\omega}\, T_{2,r}^{2\omega}\, x\, \beta_m\, D_x^{\omega-2\omega}\, (T_{1,t}^{\omega}\, G_{1,t}^{\omega}\, E_1^{\omega})^2 && \text{(Material)} \\
& + G_{2,r}^{2\omega}\, T_{2,r}^{2\omega}\, D_x^{2\omega} \sqrt{T_{1,t}^{2\omega}} \alpha_{c1}\, T_{1,t}^{\omega} (G_{1,t}^{\omega}\, E_1^{\omega})^2 && \text{(Couplant 1)} \\
& + G_{2,r}^{2\omega}\, T_{2,r}^{2\omega}\, D_x^{2\omega}\, T_{1,t}^{2\omega}\, \alpha_1\, (G_{1,t}^{\omega}\, E_1^{\omega})^2 && \text{(Transmitter)} \\
& + G_{2,r}^{2\omega}\, T_{2,r}^{2\omega}\, D_x^{2\omega}\, T_{1,t}^{2\omega}\, G_{1,t}^{2\omega}\, E_1^{2\omega} && \text{(Input)}
\end{aligned} \tag{5.19}$$

5.2.2 Nonlinearity Parameter β

The nonlinearity parameter β that is measured by the uncorrected nonlinear measurement is given by the simple relationship

$$\beta' = \frac{A_2^{2\omega}}{(A_2^{\omega})^2}. \tag{5.20}$$

A_2^{ω} and $A_2^{2\omega}$ can be broken down using Eqs. (5.17) and (5.19). The resulting Eq. (5.21) shows that the measured nonlinearity consists of six independent sources of nonlinearity:

$$
\begin{aligned}
\beta' = {} & \frac{G_{2,r}^{2\omega}}{(G_{2,r}^{\omega})^2}\,\alpha_2 && \text{(Receiver)}\\
& + \frac{G_{2,r}^{2\omega}}{(G_{2,r}^{\omega})^2}\,\frac{\sqrt{T_{2,r}^{2\omega}}}{T_{2,r}^{\omega}}\,\alpha_{c2} && \text{(Couplant 2)}\\
& + \frac{G_{2,r}^{2\omega}}{(G_{2,r}^{\omega})^2}\,\frac{T_{2,r}^{2\omega}}{(T_{2,r}^{\omega})^2}\,\frac{D_x^{\omega-2\omega}}{(D_x^{2\omega})^2}\,x\beta_m && \text{(Material)}\\
& + \frac{G_{2,r}^{2\omega}}{(G_{2,r}^{\omega})^2}\,\frac{T_{2,r}^{2\omega}\sqrt{T_{1,t}^{2\omega}}}{(T_{2,r}^{\omega}T_{1,t}^{\omega})^2}\,\frac{D_x^{2\omega}}{(D_x^{\omega})^2}\,\alpha_{c1} && \text{(Couplant 1)}\\
& + \frac{G_{2,r}^{2\omega}}{(G_{2,r}^{\omega})^2}\,\frac{T_{2,r}^{2\omega}T_{1,t}^{2\omega}}{(T_{2,r}^{\omega}T_{1,t}^{\omega})^2}\,\frac{D_x^{2\omega}}{(D_x^{\omega})^2}\,\alpha_1 && \text{(Transmitter)}\\
& + \frac{G_{2,r}^{2\omega}G_{1,t}^{2\omega}}{(G_{2,r}^{\omega}G_{1,t}^{\omega})^2}\,\frac{T_{2,r}^{2\omega}T_{1,t}^{2\omega}}{(T_{2,r}^{\omega}T_{1,t}^{\omega})^2}\,\frac{D_x^{2\omega}}{(D_x^{\omega})^2}\,\frac{E_1^{2\omega}}{(E_1^{\omega})^2} && \text{(Input)} \qquad (5.21)
\end{aligned}
$$

5.2.3 Observations

The diffraction coefficient D^{ω} is a specimen dependent, and the conversion functions G^{ω} are transducer dependent constants and therefore do not cause any variation between different measurements. Since E^{ω} and A^{ω} are the measured input and output values, it all comes down to the couplant layers, which matches the experimental observation that was made in Chap. 4.4.4.

According to Eq. (5.21), couplant layers can cause variation in two ways: Either by varying transmission coefficients T^{ω} and/or by varying nonlinearity parameters α_c. The transmission coefficients indeed do vary a lot, which can be seen in Chap. 7. On the other hand, the nonlinearity parameters α_c of the couplants are more complicated. Within one measurement $\alpha_c = \frac{A^{2\omega}}{(A^{\omega})^2} = const.$ is fulfilled, but α_c may vary between different experiments due to altered circumstances, such as pressure distribution or couplant layer thickness.

5.3 Simplified Nonlinearity Parameter β

Eq. (5.21) was developed to identify all sources of nonlinearity, but it is too complicated and contains too many unknowns to help making corrections to nonlinear measurements. For that reason, this section will consider possible simplifications to develop a practical correction method. Therefore, the following assumptions are made:

1. The clamping condition is kept perfectly unchanged during the course of one measurement. Then the acoustic reciprocity theorem states the wave transmission coefficients from transducer into material and material into transducer are the same at the same transducer: ($T^{\omega}_{1,t} = T^{\omega}_{1,r}$ and $T^{\omega}_{2,t} = T^{\omega}_{2,r}$).

2. Second harmonic generation in the couplant layer is negligible.

There are two main reasons for neglecting the couplant nonlinearity. On the one hand, the couplant layer is extremely thin which makes it seem unlikely that second harmonic generation occurs on a level, where it becomes noticeable compared to the material nonlinearity. And even if it created enough nonlinearity, it is questionable if this amount can vary enough to explain the variation of the nonlinear measurements. On the other hand, the uncertainty of the couplant terms, which where derived in Chap. 5.2.1, is very high because many assumptions had to be made. For these reasons it seems reasonable to assume that second harmonic generation in the layer can be neglected. Implementing these assumptions into Eq. (5.21) the two couplant terms drop out and the equation simplifies into

$$\begin{aligned}\beta' = \; & \frac{G^{2\omega}_{2,r}}{(G^{\omega}_{2,r})^2}\,\alpha_2 \; + \; \frac{G^{2\omega}_{2,r}}{(G^{\omega}_{2,r})^2}\,\frac{T^{2\omega}_{2}}{(T^{\omega}_{2})^2}\,\frac{D^{\omega-2\omega}_{x}}{(D^{\omega}_{x})^2}\,x\beta_m \\ & + \frac{G^{2\omega}_{2,r}}{(G^{\omega}_{2,r})^2}\,\frac{T^{2\omega}_{2}T^{2\omega}_{1}}{(T^{\omega}_{2}T^{\omega}_{1})^2}\,\frac{D^{2\omega}_{x}}{(D^{\omega}_{x})^2}\left(\alpha_1 + \frac{G^{2\omega}_{1,t}}{(G^{\omega}_{1,t})^2}\,\frac{E^{2\omega}_{1}}{(E^{\omega}_{1})^2}\right). \end{aligned} \tag{5.22}$$

With the couplant nonlinearity neglected the transmission coefficients are the only source for variation. Now it is necessary to find a way to measure these and make

appropriate corrections to the nonlinear measurements.

5.4 The Correction Method

As shown in Chap. 5.2.3 most variables in the transfer function are constant and do not cause variation. Combined with the simplifications made in the previous chapter this leaves the couplant transmission coefficients as the only possible reason for the variation of the results. Consequently, it is necessary to find a way to measure the current coupling condition.

5.4.1 Characterization of the Current System State

It is obvious, that the coupling condition must not be changed for any additional measurement that is conducted to quantify the transmission coefficient. Furthermore, another nonlinear measurement will not be any more accurate than the initial one. This leaves the two linear measurements principles that are given by Eqs. (5.1) and (5.2), resulting in four possible measurement types:

1. Through transmission from transmitter to receiver:

   $$A_2^\omega = G_{2,r}^\omega \, T_2^\omega \, D_x^\omega \, T_1^\omega \, G_{1,t}^\omega \, E_1^\omega$$

2. Through transmission from receiver to transmitter:

   $$A_1^\omega = G_{1,r}^\omega \, T_1^\omega \, D_x^\omega \, T_2^\omega \, G_{2,t}^\omega \, E_2^\omega$$

3. Echo measurement with transmitter:

   $$A_1^\omega = -(G_{1,r}^\omega \, G_{1,t}^\omega) \, (T_1^\omega)^2 \, D_{2x}^\omega \, E_1^\omega$$

4. Echo measurement with receiver:

   $$A_2^\omega = -(G_{2,r}^\omega \, G_{2,t}^\omega) \, (T_2^\omega)^2 \, D_{2x}^\omega \, E_2^\omega$$

All four measurements can be conducted with both the fundamental and the second harmonic frequency, giving a total of eight possible linear correction measurements.

Another variable is introduced at this point: θ_{12}^{ω}, which is the ratio of output to input voltage at the frequency $\boldsymbol{\omega}$, with input being on side **1** and output being on side **2**.

$$\theta_{12}^{\omega} = \frac{A_2^{\omega}}{E_1^{\omega}} = G_{2,r}^{\omega}\, T_2^{\omega}\, D_x^{\omega}\, T_1^{\omega}\, G_{1,t}^{\omega} \tag{5.23}$$

θ represents a complete measurement and will simplify future equations considerably. It is a unique representation of the coupling condition, since the transmission coefficients are the only non-constant variables in the equation. With the new notation the four measurement types can be written as

$$\theta_{12}^{\omega} = G_{2,r}^{\omega}\, T_2^{\omega}\, D_x^{\omega}\, T_1^{\omega}\, G_{1,t}^{\omega} \tag{5.24}$$

$$\theta_{21}^{\omega} = G_{1,r}^{\omega}\, T_1^{\omega}\, D_x^{\omega}\, T_2^{\omega}\, G_{2,t}^{\omega} \tag{5.25}$$

$$\theta_{11}^{\omega} = -(G_{1,r}^{\omega}\, G_{1,t}^{\omega})\, (T_1^{\omega})^2\, D_{2x}^{\omega} \tag{5.26}$$

$$\theta_{22}^{\omega} = -(G_{2,r}^{\omega}\, G_{2,t}^{\omega})\, (T_2^{\omega})^2\, D_{2x}^{\omega}\ . \tag{5.27}$$

It becomes obvious, that Eqs. (5.24) and (5.25) can be used to measure the product of both transmission coefficients, while Eqs. (5.26) and (5.27) only describe the transmission coefficient T_1 and T_2, respectively. However, it is assumed that the transmission through the couplant layers is a linear process and thus, the transmission coefficients be measured independently for each frequency.

5.4.2 Application of the Correction Measurements

Eq. (5.22) can be split into three groups, sorted by which transmission coefficients are relevant. These groups are *receiver*, *material*, and *transmitter and input*:

$$\beta' = \beta'_{receiver} + \beta'_{material} + \beta'_{t\&i} \tag{5.28}$$

$$\beta'_{receiver} = \frac{G_{2,r}^{2\omega}}{(G_{2,r}^{\omega})^2}\,\alpha_2 \tag{5.29}$$

$$\beta'_{material} = \frac{G_{2,r}^{2\omega}}{(G_{2,r}^{\omega})^2}\,\frac{T_2^{2\omega}}{(T_2^{\omega})^2}\,\frac{D_x^{\omega-2\omega}}{(D_x^{\omega})^2}\,x\beta_m \tag{5.30}$$

$$\beta'_{t\&i} = \frac{G_{2,r}^{2\omega}}{(G_{2,r}^{\omega})^2}\,\frac{T_2^{2\omega}T_1^{2\omega}}{(T_2^{\omega}T_1^{\omega})^2}\,\frac{D_x^{2\omega}}{(D_x^{\omega})^2}\left(\alpha_1 + \frac{G_{1,t}^{2\omega}}{(G_{1,t}^{\omega})^2}\,\frac{E_1^{2\omega}}{(E_1^{\omega})^2}\right) \tag{5.31}$$

The next three chapters deal with these three terms individually and suggest corrections.

5.4.2.1 Receiver Nonlinearity

For the conversion functions G being transducer dependent constants, the receiver cannot cause any variation. As long as no absolute value for the receiver nonlinearity is needed, the constant factors can be combined with the nonlinearity parameter to simplify Eq. (5.29):

$$\beta'_{receiver} = \frac{G_{2,r}^{2\omega}}{(G_{2,r}^{\omega})^2}\,\alpha_2 = \alpha'_2 \tag{5.32}$$

5.4.2.2 Material Nonlinearity

From Eq. (5.30) it can be seen, that only couplant 2 can cause variation for the material nonlinearity term. The echo measurement from Eq. (5.27) makes it possible to measure the transmission coefficients T_2^{ω} and $T_2^{2\omega}$. Therefore a change of the measurement setup is required. Transducer 1 has to be removed and two echo measurements need to be conducted with transducer 2, which used to be the receiver in the nonlinear measurement. Two echo measurements with the fundamental and second harmonic

frequency are needed:

$$\breve{\theta}^{\omega}_{1,2} = -(G^{\omega}_{2,r}\, G^{\omega}_{2,t})\,(T^{\omega}_{2})^2\, D^{\omega}_{2x} \tag{5.33}$$

$$\breve{\theta}^{2\omega}_{1,2} = -(G^{2\omega}_{2,r}\, G^{2\omega}_{2,t})\,(T^{2\omega}_{2})^2\, D^{2\omega}_{2x} \tag{5.34}$$

With Eqs. (5.33) and (5.34) inserted into Eq. (5.30), the material nonlinearity can be written as

$$\beta'_{material} = \frac{\sqrt{-\breve{\theta}^{2\omega}_{2,2}}}{-\breve{\theta}^{\omega}_{2,2}}\, D_i\; x\beta'_m\ . \tag{5.35}$$

The new variable D_i is the *diffraction correction factor* and accounts for the different diffraction coefficients of the different specimens. It is a dimensionless factor that is normalized by the first specimen, the subscript denotes the specimen number. If the diffraction correction factor is larger than 1, then the measured acoustic nonlinearity will be too large in comparison to specimen #1.

$$D_i = \frac{\left[\frac{D_x^{\omega-2\omega} D^{\omega}_{2x}}{(D^{\omega}_x)^2\sqrt{D^{2\omega}_{2x}}}\right]_i}{\left[\frac{D_x^{\omega-2\omega} D^{\omega}_{2x}}{(D^{\omega}_x)^2\sqrt{D^{2\omega}_{2x}}}\right]_1} \tag{5.36}$$

The prime at the material nonlinearity parameter β'_m denotes that it is only proportional to the absolute parameter, because several constant factors were combined with it:

$$\beta'_m = \frac{G^{\omega}_{2,t}}{G^{\omega}_{2,r}}\sqrt{\frac{G^{2\omega}_{2,r}}{G^{2\omega}_{2,t}}}\ \left[\frac{D_x^{\omega-2\omega} D^{\omega}_{2x}}{(D^{\omega}_x)^2\sqrt{D^{2\omega}_{2x}}}\right]_1 \beta_m\ . \tag{5.37}$$

The subscript 1 at the diffraction coefficient ratio denotes that this refers to specimen #1. It comes from the normalization of the diffraction correction factor in Eq. (5.36). The diffraction coefficients will not be measured in this research. Since the factor will be normalized by the first specimen, the statistical average of the measured amplitudes will be used to approximate the differences of the diffraction coefficients. The procedure is explained in more detail in Chap. 7.2.3.

5.4.2.3 Transmitter and Input Nonlinearity

The *transmitter and input nonlinearity* is given by Eq. (5.31). Considering the transmission coefficients both Eqs. (5.24) and (5.25) could be used for corrections. However, Eq. (5.24) is actually the linear part of the nonlinear measurement and therefore does not even mean an addition measurement. That way there is no need to change the measurement setup, only the amplifier has to be set to the second harmonic frequency for one measurement. Thus, the two correction measurements are

$$\tilde{\theta}^{\omega}_{1,2} = G^{\omega}_{2,r}\, T^{\omega}_{2}\, D^{\omega}_{x}\, T^{\omega}_{1}\, G^{\omega}_{1,t} \tag{5.38}$$

$$\tilde{\theta}^{2\omega}_{1,2} = G^{2\omega}_{2,r}\, T^{2\omega}_{2}\, D^{2\omega}_{x}\, T^{2\omega}_{1}\, G^{2\omega}_{1,t}\ . \tag{5.39}$$

Once Eqs. (5.31), (5.38), and (5.39) are put together the transmitter and input nonlinearity is given by

$$\beta'_{t\&i} = \frac{\tilde{\theta}^{2\omega}_{1,2}}{(\tilde{\theta}^{\omega}_{1,2})^2}\left(\alpha'_1 + \frac{E^{2\omega}_1}{(E^{\omega}_1)^2}\right) \tag{5.40}$$

with

$$\alpha'_1 = \alpha_1\, \frac{(G^{\omega}_{1,t})^2}{G^{2\omega}_{1,t}}\ . \tag{5.41}$$

5.4.3 Final Corrected Material Nonlinearity Parameter

Using Eqs. (5.28), (5.32), (5.35),and (5.40) the nonlinearity β', that was measurement with the initial nonlinear measurement, can be written as

$$\beta' \;=\; \alpha'_2 \;+\; \frac{\sqrt{-\breve{\theta}^{2\omega}_{2,2}}}{-\breve{\theta}^{\omega}_{2,2}} D_i x \beta'_m \;+\; \frac{\tilde{\theta}^{2\omega}_{1,2}}{(\tilde{\theta}^{\omega}_{1,2})^2}\left(\alpha'_1 + \frac{E^{2\omega}_1}{(E^{\omega}_1)^2}\right)\ . \tag{5.42}$$

This equation must be solved for the nonlinearity parameter β'_m to get the actual nonlinearity parameter:

$$\beta'_m \;=\; \frac{1}{xD_i}\frac{-\breve{\theta}^{\omega}_{2,2}}{\sqrt{-\breve{\theta}^{2\omega}_{2,2}}}\left[\beta' \;-\; \alpha'_2 \;-\; \frac{\tilde{\theta}^{2\omega}_{1,2}}{(\tilde{\theta}^{\omega}_{1,2})^2}\left(\alpha'_1 + \frac{E^{2\omega}_1}{(E^{\omega}_1)^2}\right)\right] \tag{5.43}$$

As shown in Chap. 4.3.3 the input nonlinearity can be neglected if a LPF is used. In this case Eq. (5.43) is reduced to

$$\beta'_m \;=\; \frac{1}{xD_i}\frac{-\breve{\theta}^{\omega}_{2,2}}{\sqrt{-\breve{\theta}^{2\omega}_{2,2}}}\left[\beta' \;-\; \alpha'_2 \;-\; \frac{\tilde{\theta}^{2\omega}_{1,2}}{(\tilde{\theta}^{\omega}_{1,2})^2}\alpha'_1\right]. \tag{5.44}$$

5.5 Summary of the New Measurement Procedure

In the beginning, the nonlinear measurement is conducted as always. Then additional measurements and calculations are necessary.

5.5.1 Additional Measurements

The linear part of the nonlinear measurement is actually the first correction measurement. The second measurement is conducted by exciting the transmitter with the second harmonic frequency. These two measurements are described by the Eqs. 5.38 and 5.39.

$$\tilde{\theta}^{\omega}_{1,2} = \frac{\tilde{A}^{\omega}_2}{\tilde{E}^{\omega}_1} = \; G^{\omega}_{2,r}\, T^{\omega}_2\, D^{\omega}_x\, T^{\omega}_1\, G^{\omega}_{1,t}$$

$$\tilde{\theta}^{2\omega}_{1,2} = \frac{\tilde{A}^{2\omega}_2}{\tilde{E}^{2\omega}_1} = \; G^{2\omega}_{2,r}\, T^{2\omega}_2\, D^{2\omega}_x\, T^{2\omega}_1\, G^{2\omega}_{1,t}$$

The other two correction measurement require a change of the experimental setup. Therefore, transducer 1 is taken off and two echo measurements are conducted with transducer 2, which used to be the receiver in the nonlinear measurement. These echo measurements need to be driven by both, the fundamental and second harmonic frequency and are specified by the Eqs. 5.33 and 5.34:

$$\breve{\theta}^{\omega}_{2,2} = -\frac{\breve{A}^{\omega}_2}{\breve{E}^{\omega}_1} = (G^{\omega}_{2,r}\, G^{\omega}_{2,t})\,(T^{\omega}_2)^2\, D^{\omega}_{2x}$$

$$\breve{\theta}^{2\omega}_{2,2} = -\frac{\breve{A}^{2\omega}_2}{\breve{E}^{2\omega}_1} = (G^{2\omega}_{2,r}\, G^{2\omega}_{2,t})\,(T^{2\omega}_2)^2\, D^{2\omega}_{2x}$$

Overall, this means three additional measurements and one change of the experimental setup.

5.5.2 Corrected Material Nonlinearity Parameter

The results of the four correction measurements can be used to obtain a more accurate value for the material nonlinearity parameter using Eq. 5.44:

$$\beta'_m \;=\; \frac{1}{xD_i}\frac{-\breve{\theta}^{\omega}_{2,2}}{\sqrt{-\breve{\theta}^{2\omega}_{2,2}}}\left[\beta' \;-\; \alpha'_2 \;-\; \frac{\tilde{\theta}^{2\omega}_{1,2}}{(\tilde{\theta}^{\omega}_{1,2})^2}\alpha'_1\right]$$

5.5.3 Limitations

The following assumptions were made to develop Eq. 5.44:

1. Transducers have a constant nonlinearity parameter $\alpha \propto \frac{A^{2\omega}}{(A^{\omega})^2}$.
2. The wave transmission coefficients from transducer into material and material into transducer are about the same: $T^{\omega}_t = T^{\omega}_r$.
3. Second harmonic generation in the couplant layer is negligible.
4. The second harmonic component in the electrical input signal is negligible, e.g. because of a LPF.
5. The transmission through the couplant layers is a linear process and thus, the transmission coefficients can be measured independently for each frequency.

5.6 Phase Relation between Fundamental and Second Harmonic

5.6.1 Difficulty

According to Eq. 5.44 one would only have to measure the transmitter and receiver nonlinearity to perfectly correct the initial nonlinearity parameter β' and obtain the material nonlinearity parameter β'_m. However, every term in the transfer function is a complex number with both an absolute value and a phase angle and therefore, simply adding or subtracting the amplitudes, thus the absolute value, is not feasible. This is actually of great importance which can be seen in Chap. 6.

The problem becomes obvious when the nonlinearity of borosilicate is measured with the PZT transmitter. If this measurement is conducted with and without a LPF and the results are compared, then the measurement with the LPF will yield a higher nonlinearity, even though the amplifier nonlinearity is filtered out. The reason for this phenomenon is that the amplifier nonlinearity ends up being almost completely phase inverse to the material nonlinearity and therefore, reducing the overall second harmonic. If the phase relation of the various second harmonic waves is not known, no correction can be made.

This yields an important conclusion: If a nonlinear measurement gives a lower value than another one, then this setup is not necessarily less nonlinear. It is also possible that the setup is highly nonlinear but different nonlinearities may just cancel out. This makes it extremely difficult to compare different setups.

5.6.2 Reference Phase

In order to compare different terms in the transfer function it is necessary to define a common reference which the phase relations can be compared to. However, there is no such thing as a constant phase shift between two waves with different frequencies. For that reason, the phase relation between second harmonic and fundamental is defined to be calculated at $\Phi_{fund} = 0°$.

Example: A FFT gives a phase of $\Phi_{fund} = 45\,°$ for the fundamental and $\Phi_{2nd} = 250°$ for the second harmonic. The phase relation is to be calculated at $0\,°$, therefore the fundamental needs to be shifted by -45 °. Since second harmonic means twice the frequency, the phase of the second harmonic needs to be shifted by $2 \cdot (-45°) = -90°$ resulting in a phase relation of $\Delta\Phi = 250° - 90° = 160°$. This can be formulated as a general equation:

$$\Delta\Phi = \Phi_{2nd} - 2\,\Phi_{fund} = 0° \tag{5.45}$$

The question is, how is the phase relation implemented in the nonlinearity parameter β. Using two generic complex numbers for the fundamental and second harmonic wave, β and the phase relation can be calculated:

$$\beta \propto \frac{A^{2\omega}}{(A^{\omega})^2} = \frac{|A^{2\omega}|\, e^{i\Phi_{2nd}}}{(|A^{\omega}|\, e^{i\Phi_{fund}})^2} = \frac{|A^{2\omega}|}{(|A^{\omega}|)^2}\; e^{i(\Phi_{2nd}-2\Phi_{fund})}\;. \tag{5.46}$$

Obviously, the phase relation that given with β is $\Delta\Phi = \Phi_{2nd} - 2\Phi_{fund}$ which is identical to what was derived in Eq. (5.45). This means, that the nonlinearity parameter β always and automatically gives a constant phase relation, no matter what the current angles of A^{ω} and $A^{2\omega}$ are.

CHAPTER VI

APPLICATION OF THE TRANSFER FUNCTION

6.1 Amplifier

6.1.1 The Experiment

Fig. 6.1 was obtained from a nonlinear measurement of Borosilicate using Lithium Niobate transducers. The output level of the amplifier was varied between 1% and 40% and the second harmonic amplitude was extracted from the direct as well as the high pass filtered signal to compare both results.

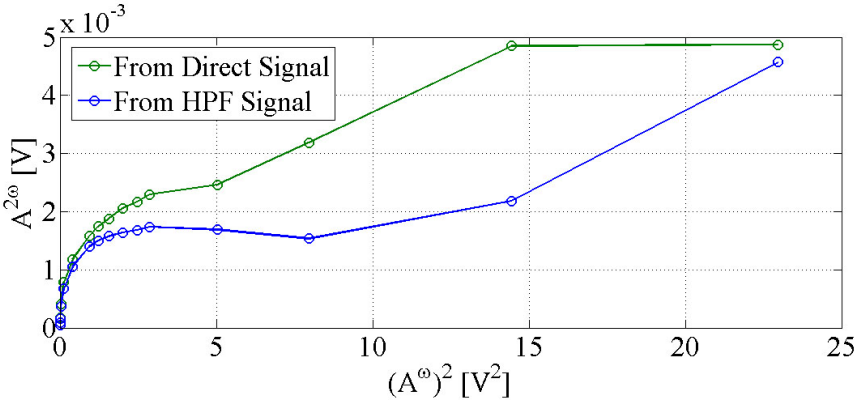

Figure 6.1: Measured Nonlinearity for Varied Output Levels

The nonlinearity plot depicted in Fig. 6.1 is distorted, even though it should yield a straight line according to $\frac{A^\omega}{(A^\omega)^2}$. If only sources with constant nonlinearity parameters were generating second harmonic waves, then the total second harmonic wave would actually give a straight line. Thus, it can be concluded that at least one source of nonlinearity has a varying nonlinearity parameter and, according to the dent at $(A^\omega)^2 = 8\,V^2$, partly cancels the others out.

This varying source is the RITEC amplifier which can be seen in Fig. 6.2. Because

of the dent, the phase difference between the second harmonic wave from the amplifier and the sum of the other second harmonic waves must be $> |90°|$ and it cannot be completely phase inverted, because in that cause there would be an output level that gives a total nonlinearity of $A^{2\omega} = 0$.

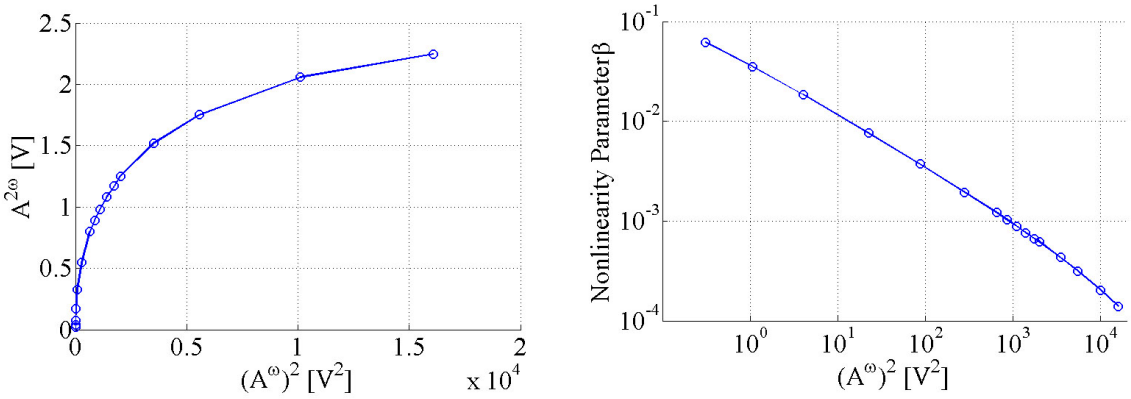

(a) RITEC Nonlinearity

(b) RITEC Nonlinearity Parameter β

Figure 6.2: RITEC Nonlinearity

6.1.2 Transfer Functions

The transfer function can be used to get the amplifier influence out of the measured results. Using Eq. (5.19) the amplifier's second harmonic wave can be subtracted from the total wave according to

$$A_2^{2\omega} - A_{input}^{2\omega} = A_{receiver}^{2\omega} + A_{material}^{2\omega} + A_{transmitter}^{2\omega} \ . \tag{6.1}$$

The indices denote the different contributions to the total second harmonic $A_2^{2\omega}$. In order to make the correction work, the relationship between the electrical input nonlinearity $E_{input}^{2\omega}$ and the contribution to the total nonlinearity $A_{input}^{2\omega}$ is needed. This relationship can be obtained from the correction measurement given by Eq. (5.24):

$$A_{input}^{2\omega} = E_{input}^{2\omega} \cdot \theta_{12}^{2\omega} \tag{6.2}$$

6.1.3 Results

The correction measurement gave an absolute value of $|\theta_{12}^{2\omega}| = 0.00217\frac{V_{output}}{V_{input}}$, but it turned out to be difficult to obtain accurate values for the phase between $E_{input}^{2\omega}$ and $A_{input}^{2\omega}$ with this measurement. Therefore, a different idea was used:

From the varying nonlinearity parameter of the amplifier depicted in Fig. 6.2(b) it becomes obvious, that the RITEC amplifier is almost 450 times more nonlinear at an output level of 1% than at 40%. For this reason it can be assumed that the total second harmonic amplitude measured at 1% output level is almost completely due to the amplifier. Thus, the phase angle was used from $\frac{A_{1\%input}^{2\omega}}{E_{1\%input}} = 0.00239 \cdot e^{i\cdot 161.8°}$. Using this phase angle and the absolute value from the correction measurement one gets

$$\theta_{12}^{2\omega} = 0.00217\frac{V_{output}}{V_{input}} \cdot e^{i\cdot 161.8°} \ . \tag{6.3}$$

The phase angle of 161.8° matches the observation that the amplifier decreases the total nonlinearity. Furthermore, note that the absolute value of the 1% ratio is only about 10% higher than the absolut value of the correction measurement. This makes sense because there should be some nonlinearity from other sources and since this ratio has proven to vary little over the whole output range. Also, these 10% difference does not make a lot of difference in the final result because the other nonlinearites finally outweigh the amplifier.

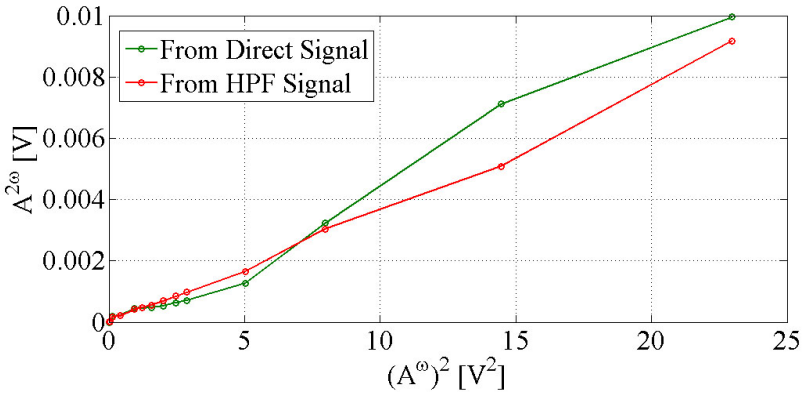

Figure 6.3: Corrected Nonlinearity

Using Eqs. (6.2) and (6.3) the electrical second harmonic from the amplifier can be transfered into the corresponding contribution at the receiver and subtracted from the total second harmonic according to Eq. (6.1). This yields the corrected plot shown in Fig. 6.3.

It is obvious that the values measured with the HPF are more accurate and give a good straight line. Also, the slope of a best fit line matches the slope pretty well, that is measured with the same experimental setup and high output levels.

The relation between the total and the corrected second harmonic wave, as well as the amplifier's contribution can be seen in Fig. 6.4(a).

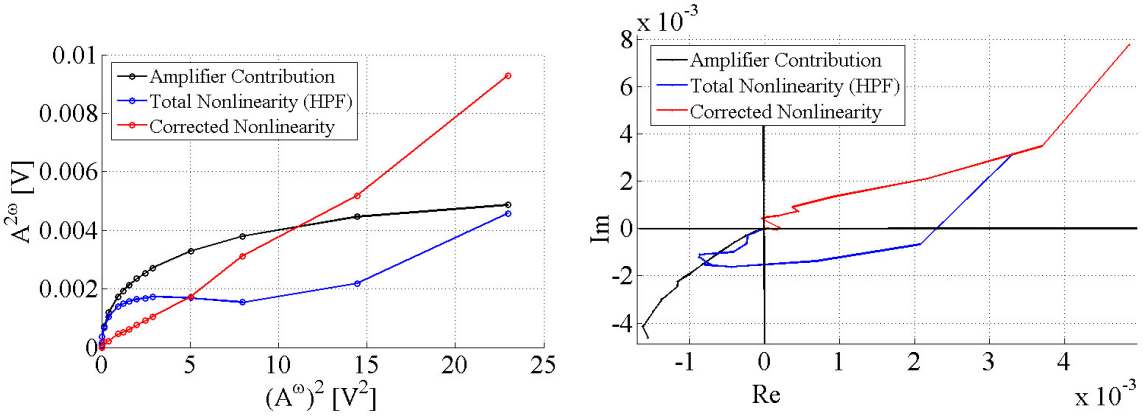

(a) Absolute Values

(b) Complex Values

Figure 6.4: Summary

Fig. 6.4(b) on the other hand uses a complex illustration of the waves to show the phase relation. That way a couple of observations can be made and confirmed:

- In the beginning, the total second harmonic almost equals the amplifier contribution.
- In the beginning, the amplifier contribution is almost phase inverted to corrected second harmonic.
- The phase angle of the corrected second harmonic is relatively constant.

- Total second harmonic converges to the corrected second harmonic for higher output levels (which was confirmed by additional measurements).

6.1.4 Conclusion

The proposed procedure to eliminate the second harmonic contribution of the amplifier works using the transfer function. The corrected second harmonic fulfills both criteria very well to be described by a nonlinearity parameter: The constant ratio of $\left|\frac{A^{\omega}}{(A^{\omega})^2}\right|$ and the constant phase angle.

6.2 Transducers

It is very hard to measure the transducer nonlinearity with the equipment that was available for this research. As soon as there are several sources of nonlinearity it becomes very difficult or even impossible to separate the second harmonic waves. This chapter deals with a few ideas about nonlinear transducers and how the contribution to the total nonlinearity could be measured.

6.2.1 Notation

The reference configuration is the experimental setup for the nonlinear through transmission experiment. This chapter only deals with the transducer nonlinearities and in order to clarify which transducer is meant, the transmitter of the nonlinear measurement will always be referred to as transmitter in this chapter, no matter if it is used to transmit or receive a wave. Consequently, the receiver will always be called receiver.

6.2.2 Transmitter Nonlinearity

For the reasons described in the previous chapter it is assumed that the couplant is linear and the the amplifier nonlinearity can be eliminated using a LPF. If the

transmitter was linear, then Eq. 5.22 can be reduced to

$$\beta' = \frac{G_{2,r}^{2\omega}}{(G_{2,r}^{\omega})^2}\,\alpha_2 + \frac{G_{2,r}^{2\omega}}{(G_{2,r}^{\omega})^2}\,\frac{T_2^{2\omega}}{(T_2^{\omega})^2}\,\frac{D_x^{\omega-2\omega}}{(D_x^{\omega})^2}\,x\beta_m \tag{6.4}$$

According to this equation neither the transmitter nor the transmitter couplant have an effect on the nonlinear measurements. Therefore, it should not have an effect if the transmitter is taken off and back on between different measurements, as long as the coupling condition at the receiver is not disturbed.

This experiment was conducted with the PZT and Lithium Niobate transmitters on Borosilicate, taking five measurements with each.

The results are clear: The variation of the transmitter measurements was about $\pm 3\%$. This means, that a second harmonic wave is induced into the material by the transmitter and thus, that the transmitter is nonlinear.

In order to compare the measurements, the same experiment was carried out with the receiver being taken off and back on without moving the transmitter. In this case the variation was about twice as high which makes sense: The receiver couplant influences the both second harmonic waves from the transmitter and material.

6.2.3 Proof of Receiver Nonlinearity

Although it is very complicated to measure transducer nonlinearities, there is a surprisingly easy way to proof that the receivers are nonlinear. All that is needed is the setup for the normal nonlinear measurement and two different receivers, PZT and Lithium Niobate in this case.

The basic idea is simple: When the nonlinear measurement is conducted a second harmonic wave excites the receiver. If the receiver is linear it will not generate any second harmonic wave that could enhance or partly cancel out the incoming second harmonic. All a linear receiver does is transform the mechanical wave into a electrical signal. That means, that both receivers should give the same nonlinearity once some

corrections are made.

6.2.3.1 Proof by contradiction

Recall the transfer function for the second harmonic at the receiver using Eqs. (5.16) and (5.18):

$$A_2^{2\omega} = G_{2,r}^{2\omega} \left(\alpha_2 \left(A_{c2}^{\omega} \right)^2 + \sqrt{T_{2,r}^{2\omega}}\, \alpha_{c2} \left(\sqrt{T_{2,r}^{\omega}}\, A_m^{\omega} \right)^2 + T_{2,r}^{2\omega}\, A_m^{2\omega} \right) \tag{6.5}$$

Assume that the receiver is linear and no second harmonic generation in the couplant occurs. Then Eq. 6.5 is simplified into

$$A_2^{2\omega} = G_{2,r}^{2\omega}\, T_{2,r}^{2\omega}\, A_m^{2\omega} \ . \tag{6.6}$$

$A_m^{2\omega}$ is the second harmonic wave coming from the material and it is constant if the transmitter is not changed during the two measurements with the Lithium Niobate and PZT receivers. The ratio of these two measurements is given by

$$\frac{\left[A_2^{2\omega}\right]_{Lith}}{\left[A_2^{2\omega}\right]_{PZT}} = \frac{\left[G_{2,r}^{2\omega}\, T_{2,r}^{2\omega}\right]_{Lith}}{\left[G_{2,r}^{2\omega}\, T_{2,r}^{2\omega}\right]_{PZT}} \ . \tag{6.7}$$

Two correction measurements are needed to account for different transmission coefficients of the couplant and conversion functions of the two receivers. Therefore, linear through transmission measurements according to Eq. 5.24 are used, both with the same transmitter settings:

$$\left[\tilde{A}_2^{2\omega}\right]_{Lith} = \left[G_{2,r}^{2\omega}\, T_2^{2\omega}\right]_{Lith} D_x^{2\omega}\, T_1^{2\omega}\, G_{1,t}^{2\omega}\, \tilde{E}_1^{2\omega} \tag{6.8}$$

$$\left[\tilde{A}_2^{2\omega}\right]_{PZT} = \left[G_{2,r}^{2\omega}\, T_2^{2\omega}\right]_{PZT} D_x^{2\omega}\, T_1^{2\omega}\, G_{1,t}^{2\omega}\, \tilde{E}_1^{2\omega} \tag{6.9}$$

The ratio of these two measurements equals the ratio that was found by Eq. 6.7:

$$\frac{\left[\tilde{A}_2^{2\omega}\right]_{Lith}}{\left[\tilde{A}_2^{2\omega}\right]_{PZT}} = \frac{\left[G_{2,r}^{2\omega}\, T_{2,r}^{2\omega}\right]_{Lith}}{\left[G_{2,r}^{2\omega}\, T_{2,r}^{2\omega}\right]_{PZT}} = \frac{\left[A_2^{2\omega}\right]_{Lith}}{\left[A_2^{2\omega}\right]_{PZT}} \tag{6.10}$$

In other words: If the receivers are linear and do not generate a second harmonic wave, then the ratio of the second harmonics in the linear measurement will be equal to the ratio of the linear correction measurement with the second harmonic frequency.

6.2.3.2 Results and Conclusion

Five measurements were conducted using a Borosilicate specimen and the Lithium Niobate transmitter, because both are supposed to be very linear. That way a potentially nonlinear receiver will be more obvious. The averages of the measurements can be seen in Table 6.1. The table also includes the results for the fundamental frequency and the corresponding measurement, which show that the high power nonlinear measurement and the low amplitude correction measurement yield similar ratios.

Table 6.1: Proof of Receiver Nonlinearity - Results

	Lithium Niobate	PZT	Ratio
Nonlinear A_2^{ω} [V]:	11.912	10.394	1.146
Correction $\tilde{A}_2^{\omega}$ [V]:	0.409	0.354	1.155
Nonlinear $A_2^{2\omega}$ [V]:	0.0604	0.0814	0.742
Correction $\tilde{A}_2^{2\omega}$ [V]:	0.01756	0.01751	1.003

The correction measurement ratio $\frac{\left[\tilde{A}_2^{2\omega}\right]_{Lith}}{\left[\tilde{A}_2^{2\omega}\right]_{PZT}} =$ is almost 1, which means that both receivers are about equally sensitive to the second harmonic frequency. However, the nonlinear measurement ratio $\frac{\left[A_2^{2\omega}\right]_{Lith}}{\left[A_2^{2\omega}\right]_{PZT}}$ yields only 0.742, which means that the nonlinearity that is measured by the PZT receiver is almost 35% higher. Therefore, at least one of the two receivers is very nonlinear.

6.2.3.3 Remarks

This only proves that at least one of the receivers is nonlinear, not which one. The problem is the phase relation: The second harmonic measured by the Lithium Niobate receiver is smaller, but a very nonlinear receiver could cancel out parts of the second harmonic wave and thus, appear more linear.

For this proof the couplant nonlinearity was assumed to negligible as in Chap. 5.3.

According to Equation 6.5 the couplant could cause the deviation that was found in this chapter as well. However, this is only possible if the identical couplant is at least 35% more nonlinear when a different transducer is used, which seems very unlikely since the transducer wear plates are very similar and the same couplant was used.

CHAPTER VII

RESULTS

For each of the seven specimen between eight and twelve measurements were conducted and each measurement included all correction measurements. The results of all these experiments are shown and discussed in this chapter.

7.1 Nonlinearity of Thermally Degraded Duplex Steel

Fig.7.1 shows the results of the nonlinear measurements without any corrections made, the second harmonic amplitude was obtained using a HPF.

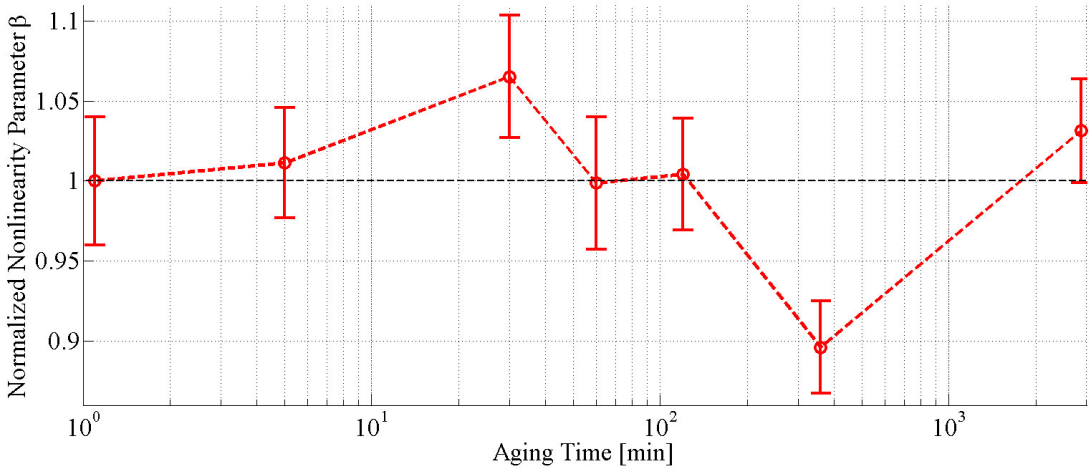

Figure 7.1: Measured Nonlinearity for the Specimen

It is obvious that the differences between the specimens are very small, only the two specimens that were thermally treated for 30 min and 360 min, respectively, stand out. For the other specimens, the error bars are too big and the differences between the specimens too small to tell a story. The longitudinal nonlinear ultrasonic technique may either not be sensitive enough to detect the damage in the specimen

or the differences are hidden in the large variation. In the latter case a way to reduce the variation would improve the resolution and therefore give clearer results.

Although the pattern of the plot cannot be explained by the precipitation of the sigma-phase, it looks suspiciously similar to the change of the hardness, shown in Fig. 3.2. If this is a real correlation, then the measured difference is probably due to influences other than an change acoustic nonlinearity.

7.2 Results of the Correction Measurements

This section analyzes the results of the correction measurements. It is split into specimen-specific results, which consider the variation between different measurements on one single specimen, and into global results, which show the differences between all seven specimens.

7.2.1 Specimen-Specific Results

7.2.1.1 Variation of the Correction Measurements

Figs. 7.2 and 7.3 illustrate the variation of the measured nonlinearity parameter β' and the correction measurements $\breve{\theta}^{\omega}_{2,2}$, $\breve{\theta}^{2\omega}_{2,2}$, $\tilde{\theta}^{\omega}_{1,2}$, and $\tilde{\theta}^{2\omega}_{1,2}$. The measurements are sorted by the nonlinearity parameter in order to see, if the correction measurements vary in a pattern that is similar to the nonlinearity parameter variation.

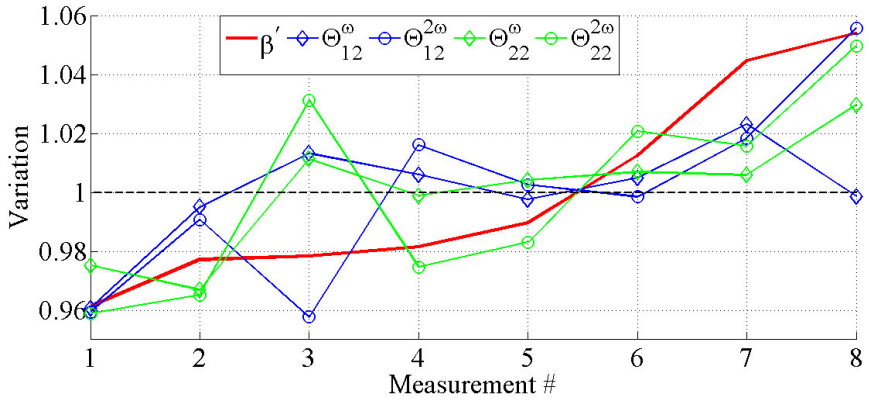

Figure 7.2: Variation of Specimen 2 Correction Measurements

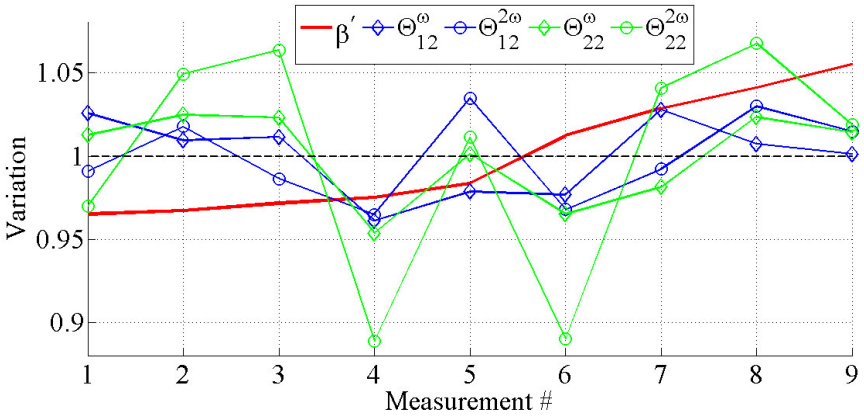

Figure 7.3: Variation of Specimen 5 Correction Measurements

From at Fig. 7.2 a correlation of β' and the correction measurements could be suspected. If a measurement of β' turns out to be lower than the average, then the correction measurements seem to show the same trend. However, there seems to be no such correlation for specimen #5 in Fig. 7.3. The results for the other specimens are something in between, some seem to show correlations, some do not. The plots for all seven specimen can be found in Appx. A.

Even though no clear correlation between β' and the correction measurements can be found, the correction measurements themselves show similar trends. Both echo measurements ($\breve{\theta}_{2,2}^{\omega}$ and $\breve{\theta}_{2,2}^{2\omega}$) vary in a similar pattern, and both through transmission experiments ($\tilde{\theta}_{1,2}^{\omega}$ and $\tilde{\theta}_{1,2}^{2\omega}$) as well. This is a rather intuitive result since it makes sense, that a bad couplant condition has a low transmission coefficient for both, the fundamental and second harmonic frequency.

7.2.1.2 Variation of the Correction Factors

The correction measurements always appear as the two correction factors $\frac{\tilde{\theta}_{1,2}^{2\omega}}{(\tilde{\theta}_{1,2}^{\omega})^2}$ and $\frac{\breve{\theta}_{2,2}^{\omega}}{\sqrt{\breve{\theta}_{2,2}^{2\omega}}}$. Therefore, it makes sense to analyze the variation of these factors because they could be constant if the correction measurements just compensate each other. The results for specimen #7 are depicted in Fig. 7.4 and it looks like there is an inverse relation

between the correction factors and the nonlinearity parameter β'. However, it only is that obvious for this specimen, the results for the other ones either show some or no trends at all, similar to the previous section. However, the through transmission

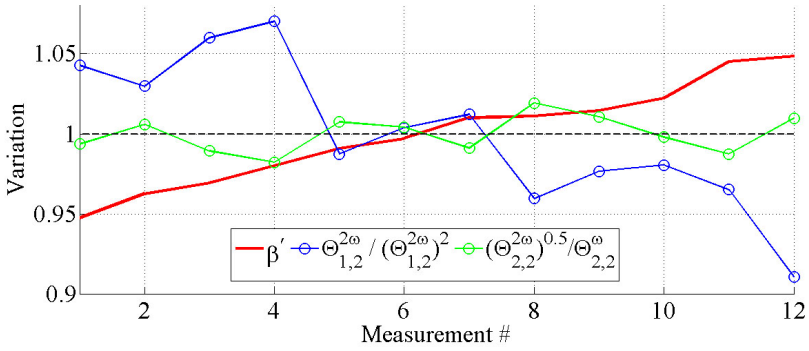

Figure 7.4: Variation of Specimen 7 Correction Factors

correction factors $\frac{\tilde{\theta}^{2\omega}_{1,2}}{(\tilde{\theta}^{\omega}_{1,2})^2}$ always show a larger variation than the correction factors, that were obtained from echo measurements. This may be due to the fact, that the former characterizes two coupling conditions, while the latter is only influenced by one. The plots for all seven specimens can be found in Appx. B.

7.2.2 Overall Results

This section compares the differences between the seven specimen, the results of all measurements are summarized in Table 7.1. Note that the nonlinearity parameters β' are not absolute values.

Table 7.1: Averages of All Specimen

Specimen	#1	#2	#3	#4	#5	#6	#7
$\beta' \cdot 1000$	1.4910	1.5080	1.5880	1.4890	1.4970	1.3360	1.5380
$\tilde{\theta}^{\omega}_{1,2}\left[\frac{mV}{V}\right]$	27.5410	27.6410	27.9330	27.7640	27.6350	27.1320	27.4310
$\tilde{\theta}^{2\omega}_{1,2}\left[\frac{mV}{V}\right]$	1.4100	1.4580	1.4730	1.5000	1.4680	1.3920	1.4610
$\breve{\theta}^{\omega}_{2,2}\left[\frac{mV}{V}\right]$	10.8970	10.7600	10.9540	10.7780	10.8050	10.7800	11.2340
$\breve{\theta}^{2\omega}_{2,2}\left[\frac{mV}{V}\right]$	70.5860	69.9940	71.5590	71.9460	71.1370	71.3100	79.1550

7.2.2.1 Overall Variation of all Measurements

The variation of the correction measurements was discussed individually for each specimen in Chap. 7.2.1.2 and did not show any clear trends. Fig. 7.5 shows the variation of the correction factors for all measurements, sorted by the deviation of the nonlinearity parameter β'. Note that this plot does not consider absolute differences between the specimen but only the deviation of each measurement from the average of the corresponding specimen.

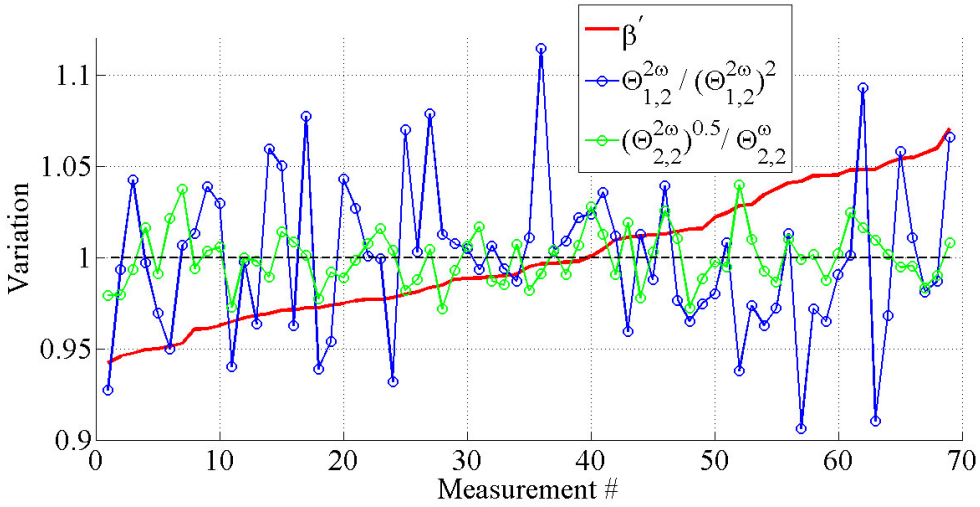

Figure 7.5: Variation of All Measurements

Still, no clear trends for the correction factors can be concluded from Fig. 7.6. However, it is conspicuous that β' values that are close to the average (between measurement #28 and #42), the correction factors seem to be pretty close to their average as well and show only little variation. This means, that these β' values would barely be corrected by the correction factors and thus, can be considered as *already correct* according to the theory.

Fig. 7.6 on the other hand shows the standard deviation for each measurement and specimen. It is obvious, that the correction measurements with the fundamental

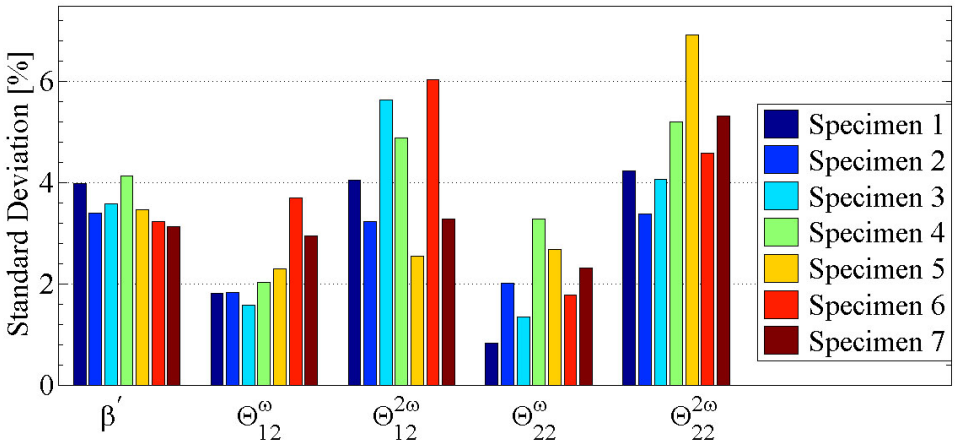

Figure 7.6: Standard Deviations of All Measurements

frequency are more accurate than the measurements with the second harmonic frequency. This is not surprising for the through transmission experiment, but it also holds true for the echo measurement with the receiver, which is a transducer that is built for the second harmonic frequency. This may indicate that the influences of the coupling condition are frequency dependent and more emphasized for higher frequencies.

7.2.2.2 Correction Measurements

Fig. 7.7 shows how much the the results for the correction measurements differ for each specimen. The two through transmission measurements, as well as two echo measurements, have similar trends again.

7.2.2.3 Correction Factors

Even though the results for the through transmission and the echo correction measurements were usually very different, both end up being very similar once the correction factors are calculated. The result is depicted in Fig. 7.8. Differences between the mean values between the correction factors are related to diffraction differences between the

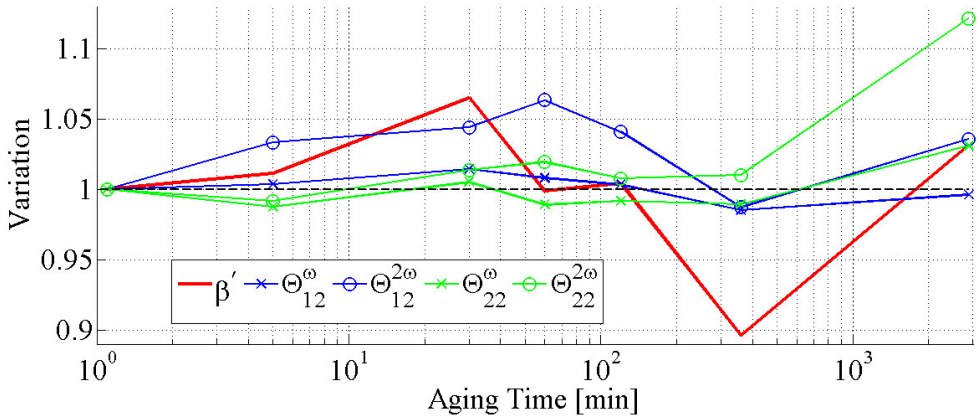

Figure 7.7: Variation of the Correction Measurements

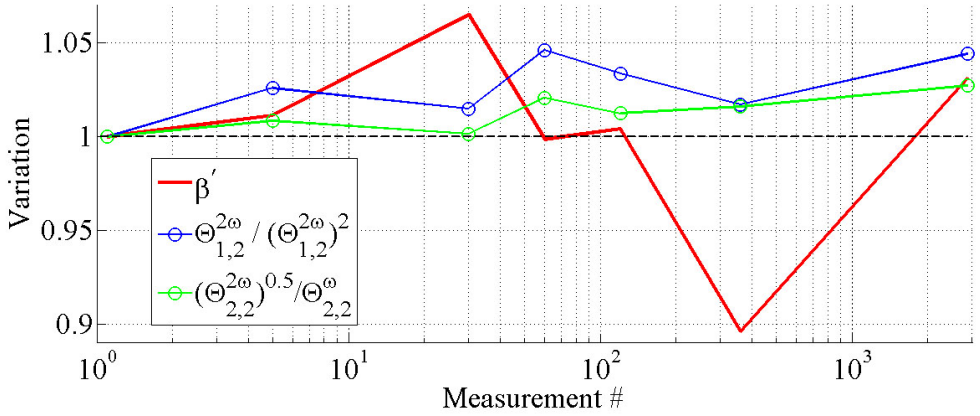

Figure 7.8: Variation of the Correction Factors

specimen, if the mean value of the transmission coefficients and the transducer convergence functions do not vary between the seven specimens. These differences can be interpreted using Eq. (5.42):

$$\beta' \;=\; \alpha'_2 \;+\; \frac{\sqrt{-\breve{\theta}^{2\omega}_{2,2}}}{-\breve{\theta}^{\omega}_{2,2}} D_i x \beta'_m \;+\; \frac{\tilde{\theta}^{2\omega}_{1,2}}{(\tilde{\theta}^{\omega}_{1,2})^2}\alpha'_1 \;.$$

As long as the acoustic nonlinearity of the material β'_m is the dominant source of nonlinearity, then $\frac{\sqrt{-\breve{\theta}^{2\omega}_{2,2}}}{-\breve{\theta}^{\omega}_{2,2}} > 1$ means that β'_m appears higher than it actually is. Such a conclusion cannot be drawn for the correction factor $\frac{\tilde{\theta}^{2\omega}_{1,2}}{(\tilde{\theta}^{\omega}_{1,2})^2}$ at this point, because depending on the phase relation the transmitter nonlinearity can either increase or decrease the total nonlinearity.

7.2.3 Diffraction Correction Factor

The correction measurements automatically account for differences of transmission coefficients and diffraction between the seven specimen. However, without the diffraction correction factor which was derived in Chap. 5.4.2.2, diffraction differences would appear as differences of the acoustic nonlinearity parameters β'_m, even though these differences are not related to a change of the acoustic nonlinearity. In order to calculate the the diffraction correction factor the diffraction coefficients of all four correction measurements are needed. Since these measurements were not part of this research, another approach is used to obtain an approximation of the diffraction correction factor. Recall Eq. (5.24) and (5.26):

$$\theta^{\omega}_{1,2} = G^{\omega}_{2,r}\, T^{\omega}_{2}\, D^{\omega}_{x}\, T^{\omega}_{1}\, G^{\omega}_{1,t}$$

$$\theta^{\omega}_{1,1} = -(G^{\omega}_{1,r}\, G^{\omega}_{1,t})\, (T^{\omega}_{1})^2\, D^{\omega}_{2x}$$

The conversion functions G are transducer dependent constants and do not vary between different specimen. It is also expected, that the average transmission coefficients for the specimens are about the same. In this case the average value of the correction measurements θ is proportional to the diffraction coefficient. This yields the relations

$$\tilde{\theta}^{\omega}_{1,2} \propto D^{\omega}_{x} \qquad \text{and} \qquad \tilde{\theta}^{2\omega}_{1,2} \propto D^{2\omega}_{x} \tag{7.1}$$

$$\breve{\theta}^{\omega}_{2,2} \propto D^{\omega}_{2x} \qquad \text{and} \qquad \breve{\theta}^{2\omega}_{2,2} \propto D^{2\omega}_{2x}\ . \tag{7.2}$$

Since the diffraction correction factors are normalized by specimen #1, it does not matter if the diffraction correction factor is calculated with the diffraction correction factors or with values, that are proportional to it.

Unfortunately this procedure does not work with the approximation that was developed for $D^{\omega-2\omega}_{x}$ in Eq. (5.12). For that reason, a different approximation is used:

$$D^{\omega-2\omega}_{x} \approx \frac{(D^{\omega}_{x})^2 - D^{2\omega}_{x}}{2\ln(D^{\omega}_{x}) - \ln(D^{2\omega}_{x})} \approx D^{2\omega}_{x} \propto \tilde{\theta}^{2\omega}_{1,2} \tag{7.3}$$

Table 7.2: Diffraction Correction Factors

Specimen	#1	#2	#3	#4	#5	#6	#7
D_i	1.0000	1.0174	1.0134	1.0251	1.0211	1.0012	1.0165

The idea behind this is, that the propagation distance in the specimen is rather short and thus, the diffraction is assumed to be small. In this case, the difference between the diffraction of a fundamental and second harmonic wave is small as well, with the diffraction of the second harmonic wave being higher. The correct diffraction coefficient is a mixture of the two coefficients for fundamental and second harmonic waves, but the influence of the fundamental is always squared because of the $\beta \propto \frac{A^\omega}{(A^\omega)^2}$ relationship. As a result, the difference between the two diffraction coefficients is decreased: If the diffraction coefficient for the fundamental wave was $D_x^\omega = 0.98$, then the squared coefficient would be $0.98^2 = 0.96$ which is closer to the lower second harmonic one.

With this approximation, the diffraction correction factors D_i can be calculated using Eq. (5.36):

$$D_i = \frac{\left[\frac{D_x^{\omega-2\omega} D_{2x}^{\omega}}{(D_x^{\omega})^2 \sqrt{D_{2x}^{2\omega}}}\right]_i}{\left[\frac{D_x^{\omega-2\omega} D_{2x}^{\omega}}{(D_x^{\omega})^2 \sqrt{D_{2x}^{2\omega}}}\right]_1} = \frac{\left[\frac{\tilde{\theta}_{1,2}^{2\omega}\ \breve{\theta}_{2,2}^{\omega}}{(\tilde{\theta}_{1,2}^{\omega})^2 \sqrt{\breve{\theta}_{2,2}^{2\omega}}}\right]_i}{\left[\frac{\tilde{\theta}_{1,2}^{2\omega}\ \breve{\theta}_{2,2}^{\omega}}{(\tilde{\theta}_{1,2}^{\omega})^2 \sqrt{\breve{\theta}_{2,2}^{2\omega}}}\right]_1} \tag{7.4}$$

The resulting diffraction correction factors are listed in Table 7.2 and plotted in Fig. 7.9. Additionally, Fig. 7.9 shows the variation for the uncorrected nonlinearity parameter β' quantitatively and both plots are obviously similar. As described in Chap. 5.4.2.2 a diffraction correction factor larger than 1 means that the acoustic nonlinearity of this specimen is actually smaller when compared to specimen #1. Also, the fact that the diffraction correction factors were obtained from only linear measurements makes it seem likely that the variation of the nonlinearity parameter β' is actually due to linear effects and not due to an increased acoustic nonlinearity of the material.

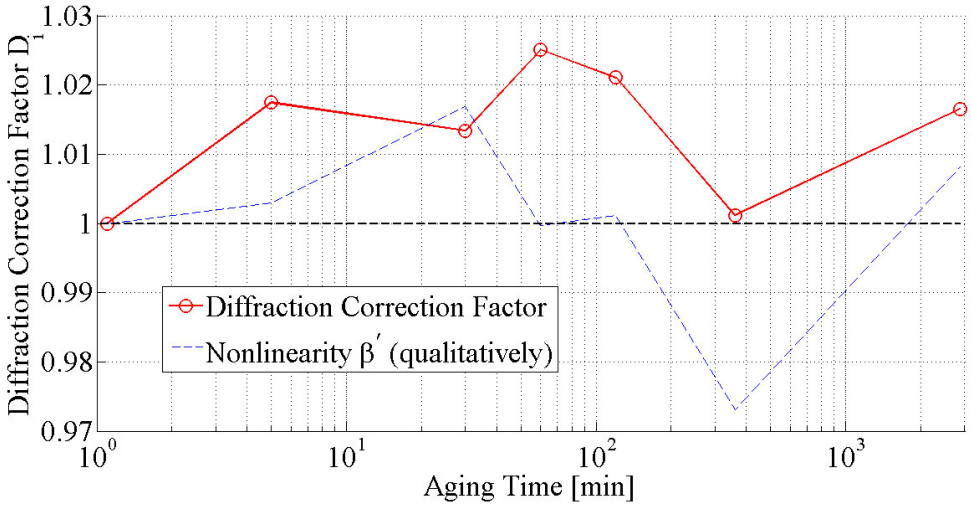

Figure 7.9: Diffraction Correction Factors

7.3 Corrected Nonlinearity of the Thermally Degraded Duplex Steel

Recall Eq. 5.44 for the corrected acoustic nonlinearity:

$$\beta'_m = \frac{1}{xD_i}\frac{-\breve{\theta}^{\omega}_{2,2}}{\sqrt{-\breve{\theta}^{2\omega}_{2,2}}}\left[\beta' - \alpha'_2 - \frac{\tilde{\theta}^{2\omega}_{1,2}}{(\tilde{\theta}^{\omega}_{1,2})^2}\alpha'_1\right]$$

Since the transducer nonlinearities could not be measured with the equipment that was available, the correction cannot be performed according to Eq. 5.44. The transducer nonlinearities could enhance or decrease the total nonlinearity, depending on the phase relation. This makes it difficult to assume any value for the transducers.

However, since the transducer nonlinearity could be added as well as subtracted, the average of all these possibilities is, that the transducers have no influence at all. It is certainly a rather big assumption, but at least the diffraction correction can be made, because Eq. 5.44 is reduced to

$$\beta'_m = \frac{1}{xD_i}\frac{-\breve{\theta}^{\omega}_{2,2}}{\sqrt{-\breve{\theta}^{2\omega}_{2,2}}}\,\beta' \,. \tag{7.5}$$

The corrected results are depicted in Fig. 7.10 and look similar to the uncorrected ones. However, the peak at 30 min is more emphasized and the drop at 360 min

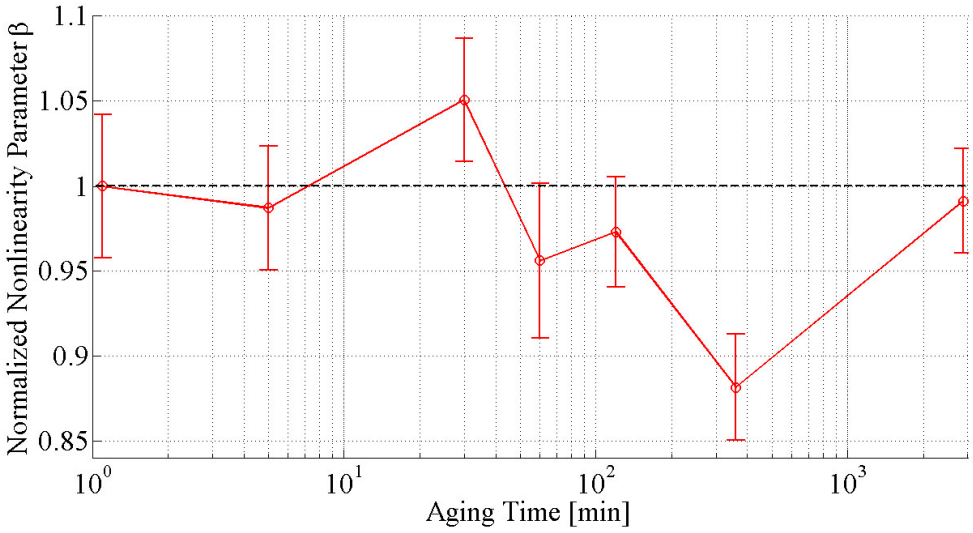

Figure 7.10: Diffraction Correction Factors

does not seem as radical anymore, because the values for 60 min, 120 min, and 48 hrs are lower than before. The variation of the nonlinearity parameter still cannot be explained with the sigma-phase.

CHAPTER VIII

CONCLUSIONS AND OUTLOOK

8.1 Conclusions

Several conclusions can be drawn from this research:

- The *individual technique* has a large influence on the results. Gradual changes with couplant usage or application force change the results considerably.

- Due to the short propagation distance ($\approx 12.1\,\mathrm{mm}$), the influences of couplant, transducers, and amplifier are very large and can overwhelm the material nonlinearity. The differences in the acoustic nonlinearity between the specimens with different thermal damage are not significant enough to be measured with this method without a very accurate correction.

- The final, uncorrected results for all specimens show a pattern that looks similar to the hardness plot. The diffraction correction factor, which is developed from only linear measurements, also shows a similar pattern. This makes it seem possible, that the differences between the nonlinearity parameters are actually related to something other than second harmonic generation in the material.

- In order to calculate the fully corrected acoustic nonlinearity parameter, the nonlinearities of the transducers and especially the phase relations need to be known. However, this could not be measured with the equipment that was available for this research.

8.2 Outlook

- As shown in Chap. 7.2.2.1 the variation of the linear measurements was higher when the second harmonic frequency was used. This may indicate that the influence of the coupling condition is frequency dependent and more emphasized at higher frequencies. This means that using a lower fundamental frequency could yield more consistent results for the nonlinear measurement. However, with a lower frequency it is not possible to use as many tone burst cycles, because the wavelength increases and the echo interferes with the transmitter earlier.

- An accurate measurement for the transducer nonlinearities is necessary to refine the correction method. This could be accomplished with an optical setup measuring the actual oscillation of the transducer surface. The transducer could be attached to a transparent specimen like Borosilicate to simulate the specimen's resistance.

- For the correction method it would be very helpful, if accurate values for the acoustic nonlinearity could be obtained. Knowing what is correct would make it easier to find possible sources of error in the correction method. There are basically three methods that may yield better values for the acoustic nonlinearity:

    1. The most promising way is to fabricate new specimens with different thicknesses for each hold time. With various wave propagation distances everything but the material nonlinearity ends up being a constant and the acoustic nonlinearity could be measured very reliably.
    2. Real single crystal transducers, such as Quarts or Lithium Niobate, could be used. Maybe the transducer nonlinearity is not due to the Lithium Niobate crystals inside the transducer case, but due to how they are mounted

by the manufacturer.

3. A different technique, such as the resonance frequency shift, could be used to measure the acoustic nonlinearity parameter.

APPENDIX A

VARIATION OF CORRECTION MEASUREMENTS

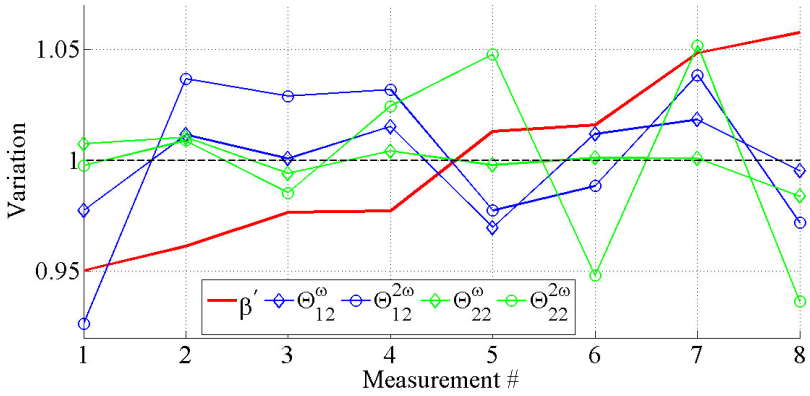

Figure A.1: Variation of Specimen 1 Correction Measurements

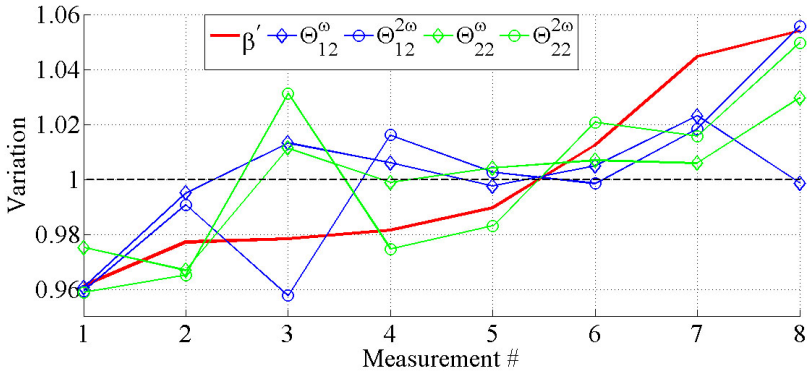

Figure A.2: Variation of Specimen 2 Correction Measurements

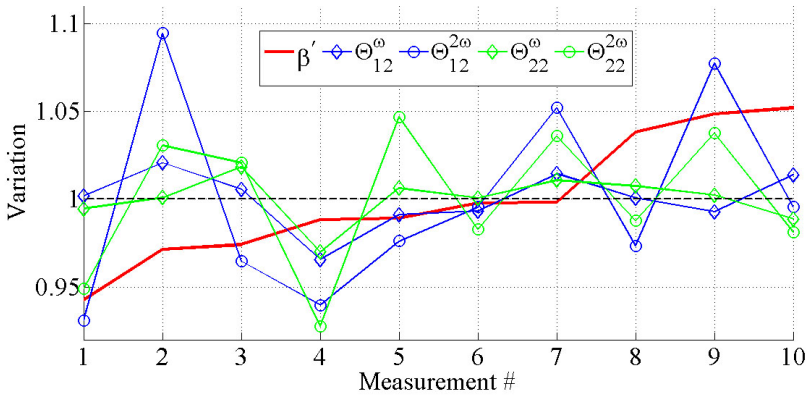

Figure A.3: Variation of Specimen 3 Correction Measurements

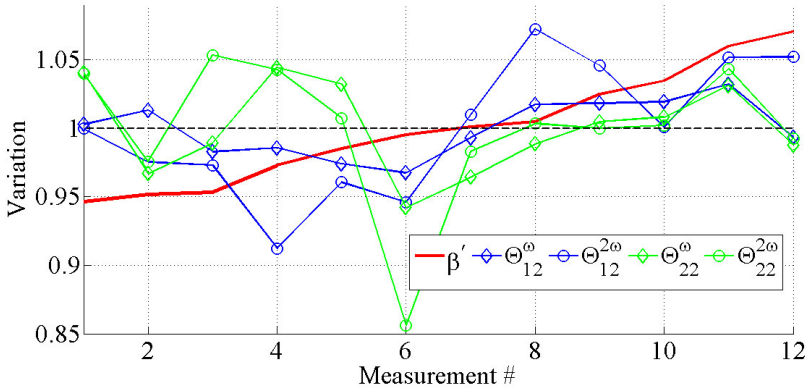

Figure A.4: Variation of Specimen 4 Correction Measurements

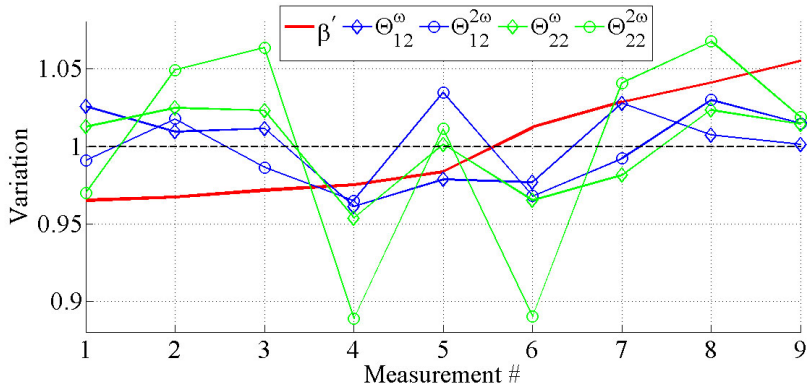

Figure A.5: Variation of Specimen 5 Correction Measurements

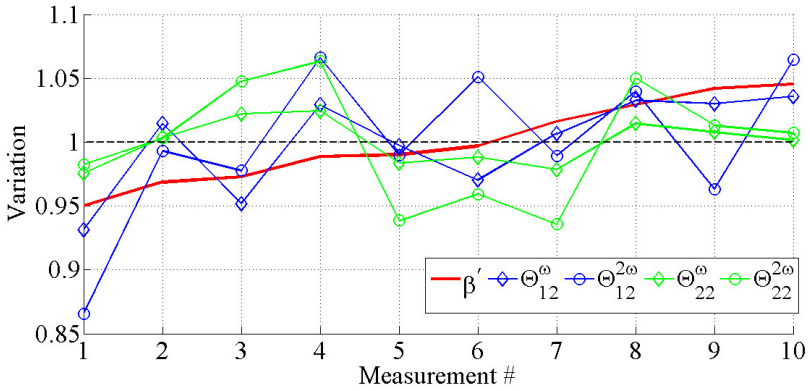

Figure A.6: Variation of Specimen 6 Correction Measurements

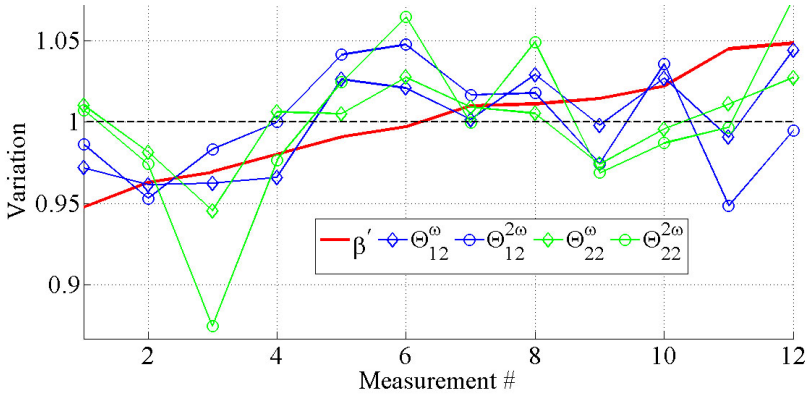

Figure A.7: Variation of Specimen 7 Correction Measurements

APPENDIX B

VARIATION OF CORRECTION FACTORS

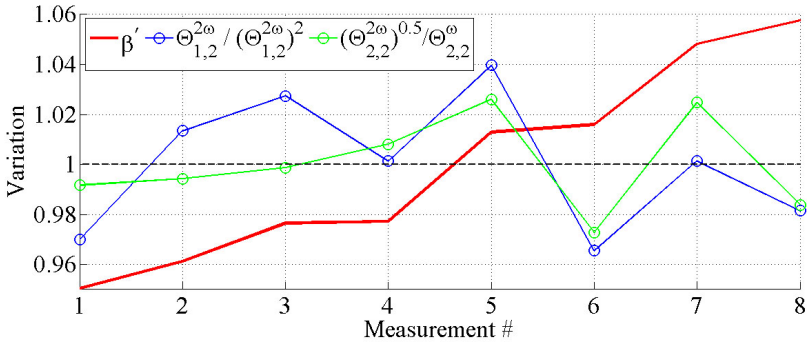

Figure B.1: Variation of Specimen 1 Correction Factors

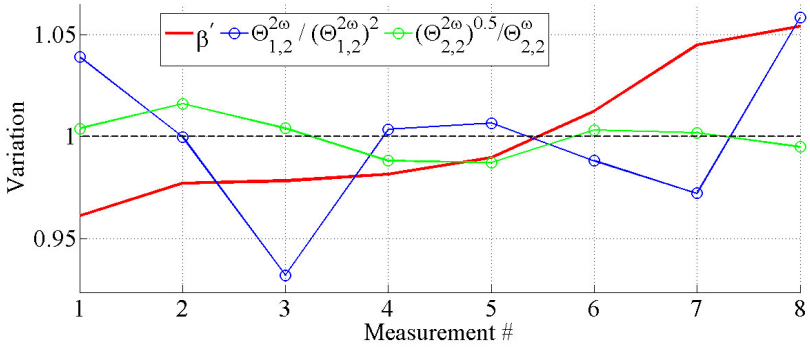

Figure B.2: Variation of Specimen 2 Correction Factors

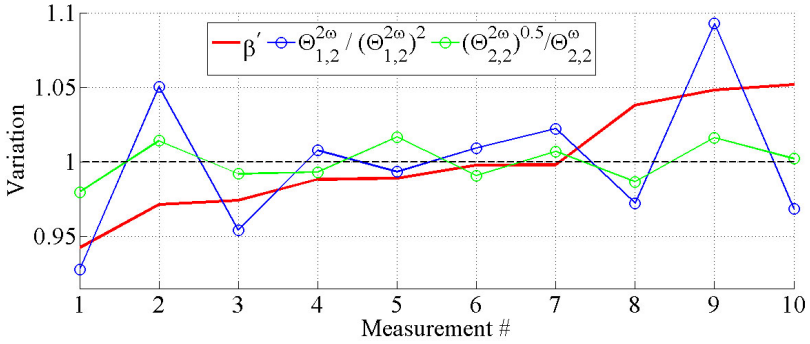

Figure B.3: Variation of Specimen 3 Correction Factors

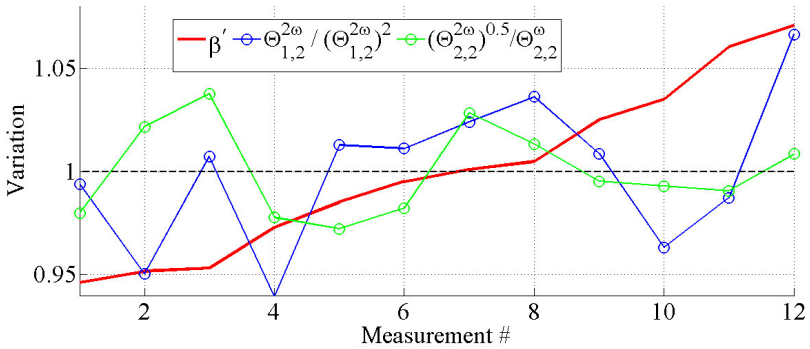

Figure B.4: Variation of Specimen 4 Correction Factors

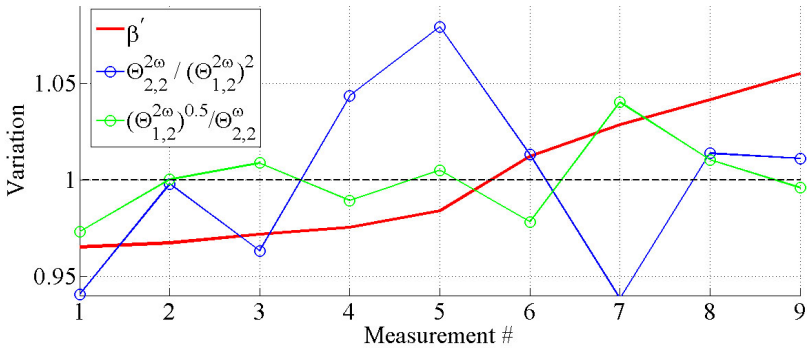

Figure B.5: Variation of Specimen 5 Correction Factors

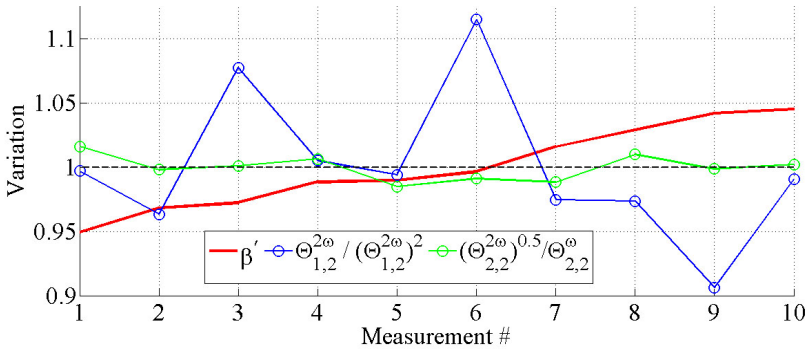

Figure B.6: Variation of Specimen 6 Correction Factors

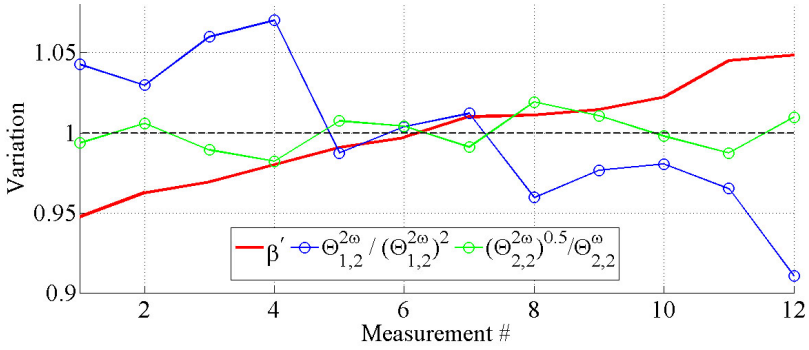

Figure B.7: Variation of Specimen 7 Correction Factors

REFERENCES

[1] Baby, S., Kowmudi, B. N., Omprakash, C., Satyanarayana, D., Balasubramaniam, K., and Kumar, V., "Creep damage assessment in titanium alloy using a nonlinear ultrasonic technique," *ScienceDirect*, vol. 59, 2008.

[2] Cantrell, J. H. and Yost, W. T., "Effect of precipitate coherency strains on acoustic harmonic generation," *Journal of Applied Physics*, vol. 81, pp. 2957–2962, 1997.

[3] Cantrell, J. H. and Yost, W. T., "Determination of precipitate nucleation and growth rates from ultrasonic harmonic generation," *Applied Physics Letters*, vol. 77, pp. 1952–1954, 2000.

[4] Chen, T., Weng, K., and Yang, J., "The effect of high temperature exposure on the microstructural stability and toughness property in a 2205 duplex stainless steel.," *Materials Science and Engineering*, vol. 338, pp. 259–270, 20002.

[5] Jiang, Z., Chen, Huang, H., and Liu, "Grain refinement of cr25ni5mo1.5 duplex stainless steel by heat treatment.," *Materials Science and Engineering*, vol. 363, pp. 263–267, 2003.

[6] Jr., R. E. G., *Ultrasonic Investigation of Mechanical Properties.* Academic Press, 1973.

[7] Kim, J.-Y., Jacobs, L. J., Qu, J., and Littles, J. W., "Experimental characterization of fatigue damage in a nickel-base superalloy using nonlinear ultrasonic waves," *Journal of Acoustical Society of America*, vol. 120, pp. 1266–1273, 2006.

[8] Ruiz, A., Ortiz, N., Cerren, H., and Rubio, C., "Utilization of ultrasonic measurements for determining the variations in microstructure of thermally degraded 2205 duplex stainless steel," *Journal of Nondestructive Evaluation*, vol. 28, pp. 131 – 139, 2009.

[9] Sieurin, H. and Sandstrm, R., "Sigma phase precipitation in duplex stainless steel 2205," *Materials Science and Engineering*, vol. 379, pp. 259–270, 2004.

[10] Solomon, H., Devine, T., and R.A.Lura, "Duplex stainless steel," *American Society for Metals, Metal Park*, pp. 553–652, 1983.

[11] Sun, L., Kulkarni, S. S., Achenbach, J. D., and Krishnaswamy, S., "Technique to minmize couplant-effect in acoustic nonlinearity measurements," *Journal of Acoustical Society of America*, vol. 120, pp. 2500 – 2505, 2006.

[12] Treiber, M., "Characterization of cement-based multiphase materials using ultrasonic wave attenuation," Master's thesis, Georgia Institute of Technology, 2008.